FCTUC FACULDADE DE CIÊNCIAS E TECNOLOGIA
UNIVERSIDADE DE COIMBRA

DEPARTAMENTO DE ENGENHARIA MECÂNICA

Influence of temperature in the deep drawing of 6xxx aluminium alloys

Submitted in Partial Fulfilment of the Requirements for the Degree of Master of Science in Mechanical Engineering in Production Systems Speciality

Author
José Paulo Pinto Abrantes

Advisors
Marta Cristina Cardoso de Oliveira
Hervé Laurent

Jury

President	**Professora Doutora Ana Paula Betencourt Martins Amaro** **Professora Auxiliar da Universidade de Coimbra**
Vowels	**Professor Doutor José Luís de Carvalho Martins Alves** **Professor Auxiliar da Universidade do Minho**
Advisor	**Professora Doutora Marta Cristina Cardoso de Oliveira** **Professora Auxiliar da Universidade de Coimbra**

Université de Bretagne-Sud

UBS Université de Bretagne-Sud

LIMATB Laboratoire d'Ingénierie des MATériaux de Bretagne

Coimbra, July, 2014

“The only difference between me and a madman is that I am not mad.”

Salvador Dali

ACKNOWLEDGEMENTS

The work presented was only possible due to the collaboration and support of some people, for which I want to show my gratitude.

My supervisors, Prof. Dr. Luís Menezes and Prof. Dr. Hervé Laurent, for given me the opportunity to join this project and this team, with all the support given.

My adviser Prof. Dr. Marta Oliveira, for all the hours without sleeping, for all the concern for a good work, for the visit in France, and for all the suggestions and discussions regarding the research, a great thank you for helping me in this journey, without you this would not be possible.

Jeremy Cöer and Anthony Jegat, for your availability in helping me with all my problems and doubts, always with good attitude.

To Vasco Simões, for all the guidance and help, beside all the problems, a great friend that I will keep for life.

To my friends in Lorient, that made my stay and my work more pleasant.

To my closest friends in the Department, Jota, Ruca, Edu, Maça, Leandro, Ana Raquel, for helping me through this five years, and for making me a better person everyday, a great thank you guys and wish you all the best.

To all my friends, especially Granjo, Telles, Henrique, Guincho, Guerra, Brito, Sofia Lemos and Teresa Maia, for not letting me go through this path on my own, and always being present for the greatest and the worse moments, thank you for the moments we've shared.

To my parents and sister, and also my family, for all the support during all my life, nothing of this would be possible without you. Thanks for having given me the better life that anyone could desire.

To Joana Genésio, for all the late talks, for not having given up on us, even with the distance, for encouraging me to pursuit always the best for me and my life, for all the support, the laughs, the smiles, the hugs, for making me a better person, there are no words to match what you have done.

Without all of you, none of this would be possible.

For all, a great Thank you.

RESUMO

Nos dias de hoje os processos de estampagem são uma componente de grande importância para a indústria. As ligas de alumínio são dos materiais mais utilizados na indústria automóvel. No entanto, as da série 5xxx são apenas usadas para os painéis interiores, uma vez que apresentam defeitos de superfície, enquanto as da série 6xxx são utilizadas nos painéis exteriores das viaturas. O principal objectivo deste estudo é caracterizar mecanicamente ligas da série 6xxx e avaliar as potencialidades de recorrer à sua estampagem a quente, de modo a tentar dar resposta a um conceito de utilização de apenas uma liga de alumínio na indústria (6xxx), com consequentes impactos positivos do ponto de vista económico e de reciclagem.

O estudo descrito neste trabalho resulta de uma parceria entre o CEMUC e o LIMATB, com o objectivo de estudar a influência da temperatura no processo de estampagem de taças cilíndricas da série 6016-T4 e 6061-T6, tendo sido estudadas duas temperaturas: ambiente e 200ºC. O estudo envolveu a realização de ensaios experimentais de estampagem de taças cilíndrica e a simulação do processo, admitindo condições isotérmicas. Os parâmetros analisados foram a evolução da força do punção com o seu deslocamento, a evolução da espessura ao longo da taça e o perfil das orelhas de estampagem. O retorno elástico foi estudado experimentalmente, com o auxílio do teste Demeri. Todas as simulações numéricas foram realizadas com o programa DD3IMP,e a caracterização dos materiais foi realizada com o programa DD3Mat. A análise experimental foi realizada no LIMATB.

Os resultados permitem concluir que a realização da estampagem a 200ºC conduz a uma redução da força de estampagem e do retorno elástico, maioritariamente para o 6061-T6.

Palavras-chave: Ligas de alumínio, Estampagem, Temperatura, Retorno elástico, Simulação numérica

ABSTRACT

Nowadays the deep drawing processes are a component of huge importance to industry. The aluminium alloys are one of the most used materials in the automotive industry. However, the 5xxx alloys are only used in inner panels, since they present superficial defects, while the 6xxx alloys are used in the outer panels of cars. The main goal of this study is to characterize the mechanical behaviour of 6xxx alloys and evaluate the potential of using warm deep drawing, in order to respond to a single material use concept of aluminium alloys in industry (6xxx), with positive consequences regarding the economic and recyclability point of view.

The study presented in this work results from a partnership between the CEMUC and the LIMATB, with the purpose of studying the influence of temperature in the deep drawing process of cylindrical cups for the 6016-T4 and 6061-T6 alloys, based on two different temperatures: room temperature and 200ºC. This work involved performing deep drawing of cylindrical cups experimental tests and the numerical simulation of the process, assuming isothermal conditions. The analysed parameters were the evolution of the punch force with the punch displacement, the evolution of thickness along the cup's wall and the ears profile. The springback was study experimentally, with the help of the Demeri test. All the numerical simulations were performed using the in-house code DD3IMP, and the material characterization was performed using the DD3Mat. The experimental analysis was accomplished in LIMATB.

The results allow us to conclude that performing the deep drawing at 200ºC leads to a punch force and springback reduction, mainly for the 6061-T6.

Keywords Aluminium alloys, Deep Drawing, Temperature, Springback, Numerical analysis.

CONTENTS

LIST OF FIGURES

LIST OF TABLES

SYMBOLOGY AND ACRONYMS

Symbology

α - Angle with radial/rolling direction

β – Limit drawing ratio

$\bar{\varepsilon}^p$ – Equivalent plastic strain

Δr – Planar anisotropy coefficient

d_{punch} - Punch diameter

D_{max} - Maximum sheet diameter

E – Young's modulus

F, G, H, L, M, N – Hill'48 anisotropy criterion parameters

r_α –Plastic anisotropy coefficient for α

r_0, r_{45}, r_{90} – Plastic anisotropy coefficients

Y_0, Y_{sat}, C_y – Voce law material parameters

Y_f – flow stress

Acronyms

AA 5754-O – Aluminium alloy 5754-O

AA 6016-T4 – Aluminium alloy 6016-T4

AA 6061-T6 – Aluminium alloy 6061-T6

CEMUC – Centro de Engenharia Mecânica da Universidade de Coimbra

DD3IMP – Deep Drawing 3d IMPlicit code

DD3Mat – Deep Drawing 3D MATerials Parameters Identification code

LDR – Limit Drawing Ratio

LIMATB – Laboratoire d'Ingénierie des MATériaux de Bretagne

RT – Room temperature

RD – Rolling direction

DD – Diagonal direction

TD – Transverse Direction

1. INTRODUCTION

Aluminium is the lead non-ferrous metal more used nowadays. Known as a truly versatile engineering material, aluminium and its alloys are used in applications from aerospace to automobile industry, building, sports and many others. Characteristics as lightness, good formability, high strength, good corrosion resistance and recycling potential (100%), make it the most used material to replace heavier materials, such as steel, in many industries. One of the many reasons why it is used in the automobile industry is due to its ability to save weight. However, for some applications its use is still limited due to the poor formability of some alloys.

The lightweight, providing a huge mass reduction in body parts, and the high strength stiffness to weight ratio [Ghosh et al., 2014], are the main reasons to use aluminium. However, the cost of aluminium alloys, which is twice higher than that of steel, and their poor formability at room temperature, which is typically 2/3 of that of steel, as reported by Ayres and Wenner (1979) (in [Ghosh et al., 2014]), puts them in a disadvantage position facing the future.

1.1. Aluminium Alloys 5xxx and 6xxx

Regarding the different type of aluminium alloys that exist nowadays, they are typically group in two big groups: aluminium alloys sensitive to heat treatment, as 2xxx, 6xxx and 7xxx; and aluminium alloys not sensitive do heat treatment, as 1xxx, 3xxx and 5xxx [TN, 2004]. The most commonly used in automotive industry are de 5xxx and 6xxx series.

Regarding the 5xxx series, they are used to produce inner panels due to the excellent deep drawing performance, formability and high resistance. However, this series presents high values of springback and surface defects that enable their used in outer panels [Simões, 2012].

The focus of the study is the 6xxx group, trying to develop this alloy for inner panel applications, in response to the single material use concept. 6xxx series are characterized by the presence of magnesium (Mg) and silicium (Si) as major alloying elements, combining the best of tensile strength and ductility. They are commonly used by

the automobile industry due to the possibility of being heat treatable and to the fact that do not suffer from the presence of stretcher lines, which affects the surface quality of components produce with other aluminium alloys. For this reason, this series (6xxx) is mainly used for external car body components, while 5xxx alloys, are used for internal car body components, due to its higher strength and to the fact that surface quality is not important [Gosh et al., 1994]. Nevertheless, there is some controversy in literature about this subject. Burger et al. (1995), Ghosh et al. (1994) and Fridlyander et al. (2002) claim that the 6xxx series alloys have the advantage of being free of Luders bands, which allows a high surface quality. This arises from the lower Mg content compared to the 5xxx series. Other solute elements such as Si and Cu are either energetically bound to Mg in the form of coherent clusters or have too low diffusion rates to enable the formation of effective solute atmospheres that pin dislocations [Ghosh et al. (2014)]. However, Rashkeev et al. (2002) claims that this series, with some strain rate range and loading paths, also presents this effect. Trying to overcome this problem, the warm workability of aluminium and its alloys has been of both technical and scientific interest in the last decade. In this context, the goal of this study was to study the influence of temperature in the deep drawing process of cylindrical cups for the 6016-T4 and 6061-T6 alloys. Following previous works, the component selected was a cylindrical cup, which allows the analysis of the springback effect using the split-ring test [Coër, 2013].

1.2. Influence of heat treatment in 6xxx alloys

6xxx alloys have the advantage of being heat treatable. After solution heat treatment they show low yield strength (<130 MPa) and good formability, which results in low springback and relative ease for production of complex parts with high dimensional accuracy [Ghosh et al., 2014].

According to Park (1986), "These heat treatable 6xxx type alloys are well known for their useful strength and toughness properties in both T4 and T6 tempers and are generally considered as having relatively good corrosion resistance which makes them advantageous even over the very high strength and more expensive 7xxx alloys which sometimes can exhibit more corrosion than 6xxx alloys."

Concerning the two types of heat treatments used, T4 and T6, Park (1986) also states that the T4 condition refers to a solution heat treated and quenched condition

naturally aged to a substantially stable property level, whereas the T5 and T6 tempers refer to a stronger condition produced by artificially aging typically at temperatures of 220°-350° or 400°C, for a typical period of hours. In fact, according to Mahathaninwong (2012): "T6 heat treatment is one of the major factors to enhance mechanical properties of the alloy through an optimization of both the solution heat treatment and the artificial aging conditions".

2. DEEP DRAWING PROCESS

The deep drawing process is widely used nowadays in a variety of industrial areas such as automobile, aerospace and packaging. The process consists in forming complex and not expandable sheet metal parts from a plane surface, but also serves as a basic test for the sheet metal formability.

As Figure 2.1 shows, this process involves three tools: blank-holder, die and punch. Each one of the tools has a specific task: the blank-holder presses the blank against the die, avoiding wrinkling; the die defines the shape of the final product; and the punch drives the blank into the die's cavity.

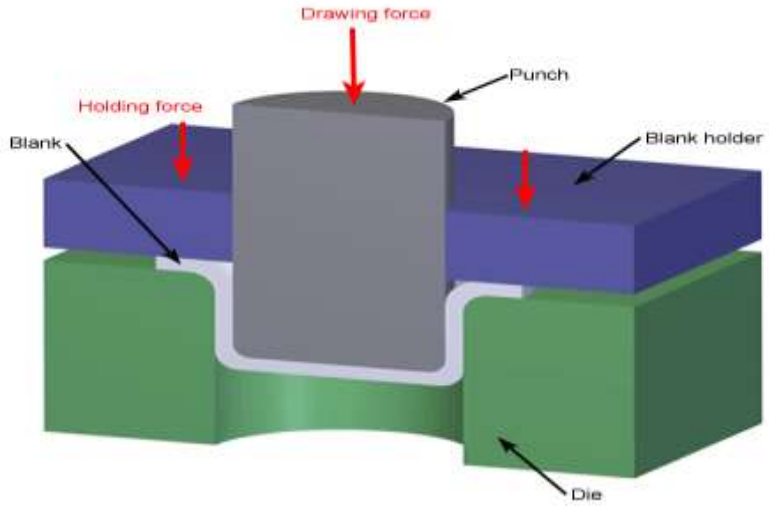

Figure 2.1 - Deep drawing process of a cylindrical cup.

According to Raju et al. (2010), for cylindrical components: "During the course of deep drawing, the following five processes take place. They are: 1) pure radial drawing between the die and blank holder, 2) bending and sliding over the die profile, 3) stretching between the die and the punch, 4) bending and sliding over the punch profile radius, and 5) stretching and sliding over the punch face."

The following sections are based on the literature review and present a description of the phenomena related with the deep drawing process, as well as influential parameters.

2.1. Springback phenomenon

The main problem regarding the deep drawing process considering the aluminium alloy is the springback phenomenon. This phenomenon is the main responsible for the change of shape of the final product, as well as warping. A good prediction of the springback is a huge help to figure the right adjustments that have to be made in order to get the exact final shape desired. The past years many studies have focused in reducing this phenomenon, most of them through warm deep drawing [Coër, 2013; Gosh et al., 2014], which show that a significant decrease can be found.

Figure 2.2 – From left to right, experimental drawn cup, cut rings and springback after splitting [Laurent et al., 2008].

Springback is defined as the elastic recovery after releasing a part from the die and it happens due to the redistribution of elastic energy gained during the process [Malavolta, 2008; Chen et al., 2005]. This phenomenon will change the final shape of the part, making the prediction of the final geometry after the springback very difficult. Therefore, it is extremely important to find a way to predict the right behaviour/influence of this phenomenon, in order to reduce the amounts of scrap. As referred by Moon et al. (2003) springback is influenced by several factors, such as sheet thickness, elastic modulus, yield stress, work hardening exponent, etc.; the inaccurate definition of the dependence of springback on the above parameters can cause productivity loss due to scrapping or reworking. Over the last years, several test have been proposed to measure springback effects. However, regarding the cylindrical cups only one test is suitable, which is the "split-ring" test, similar to the Demeri Benchmark test (see Figure 2.2). This process consists in four steps: (a) Deep drawn a cylindrical cup from a circular blank with a constant blank-holder force; (b) Cut a circular ring from the mid-section of the drawn cup;

(c) Split the ring along a certain direction, to release residual stresses introduced from drawing operation, and (d) Measure the opening of the ring (springback) [Chen et al., 2005].

2.2. Influential parameters in the process

In order to improve the results of the deep drawing process a better understanding of the parameters involved, such as lubricant conditions, forces and stress states, effect of temperature, blank-holder force, tools geometry and deep drawing speed is necessary. In this work the effect of temperature is the main parameter studied, but also some of the other parameters are succinctly described in the following sections.

2.2.1. Effect of temperature

In order to improve the workability of the alloys and also to improve the process and the parameters involved in it, former studies focused in the influence of temperature in the deep drawing process and its advantages concerning the final geometry, including springback, and the consumed energy (i.e. force-displacement curves).

As Gosh (2014) concluded for cylindrical components: "among the investigated parameters, the effect of temperature was significant principally on the force-displacement response of the materials. The number of ears remained unchanged with increasing temperature but the amplitude of ears was reduced".

Regarding the final geometry of the deep drawn component the temperature has a small influence in the final result. In contrast, considering the springback effect, the temperature has a huge influence in this phenomenon, as the springback decreases significantly for tests at 200ºC [Coër, 2013]. Therefore, increasing the drawing temperature from room temperature (RT) to 250°C does not change the type of anisotropic behaviour, but reduces the height of the ears showing that the material behaves more isotropically [Gosh, 2011]. Although, in the work of Coër (2013) is quite noticeable that the cup's height decreases with the increase of temperature, but the amplitude of the ears does not suffer a decrease, as it was stated by Gosh (2011).

Regarding the temperature of the tools, Moon et al. (2012) concluded that a hot die is very effective in reducing the springback amount. Also, the combination of a hot die

with a cold punch can reduce the amount of springback up to 20%, when compared to conventional room temperature bending test.

2.2.2. Forces

Figure 2.3 presents the forces that the blank is submitted in the deep drawing process. During the deep drawing, the forces occurring are: i) Bending at the radius; ii) Friction between blank-holder and sheet metal, die and sheet metal and punch and sheet metal; iii) Compression at flange area [Ramesh et al., 2013].

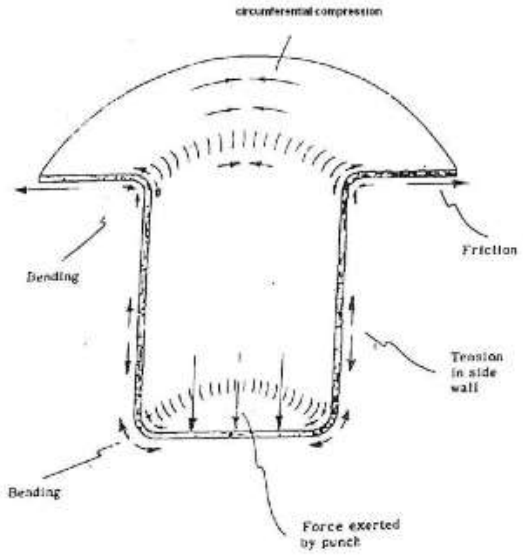

Figure 2.3 – Forces during the deep drawing process [Ramesh et al., 2013].

The cup's bottom is only submitted to compression, due to the force applied by the punch. When the blank is pushed into die's cavity, the flange area (located in the gap between the blank-holder and die) is strongly compressed in the circumferential direction, while is pulled in the radial direction, in order to reduce the radius to be able to fit the die's cavity. This reduction is complemented by the increasing of the cup's height, being dependent of the anisotropic behaviour of the material, which dictates the ears formation.

Regarding the stress states that the cup is submitted, Figure 2.4 gives some more details about their location. In this case, and as state by Simões et al. (2013), "the cup's bottom is mainly submitted to a biaxial stress state, the flange area to a shear state and the cup's wall is mainly submitted to plane strain state, which tends to a shear state when the ironing process occurs".

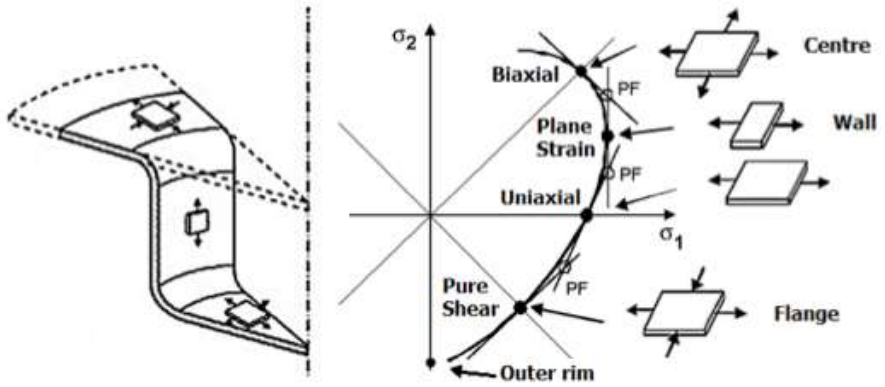

Figure 2.4 - Stress states and their location in the cylindrical cup [Alves, 2003; van der Boorgaard et al., 2006].

2.2.3. Others parameters

The deep drawing process of cylindrical cups is also sensitive to others parameters, as the lubricant conditions, the blank-holder force, the limit drawing ratio, etc.

Regarding lubricant conditions, previous studies [Simões, 2012] shown that it is not imperative to measure the amount used in the deep drawing process of cylindrical cup's, as long as some lubricant exists in the blank and in the tools involved in the process (blank-holder and die).

There are several studies that discuss the effect of the blank-holder force (BHF) on the deep drawing process. As stated by Ramesh et al. (2013): "Higher the BHF, higher is the frictional forces between the blank and blank holder, so higher the loads required for drawing operation and higher the strains developed in the cup walls between the die and punch, thereby reducing thickness of the section". Still on the same subject, Reddy et al. (2012) states that the force exerted by the blank-holder on the sheet supplies a blank holding force that controls the metal flow. This restraining action is largely applied through friction, concluding that, if the value of friction coefficient is lower, the role of the blank-holder is also inferior. On the other hand, a higher value of the blank-holder forces leads to an increase of the cup's height.

The limit drawing ratio (LDR), β, is defined as the ratio of the maximum sheet diameter, D_{max}, and the punch diameter, d_{punch}, just before an edge crack occurs [Ozek et al., 2009]. It is defined by:

$$\beta = \frac{D_{max}}{d_{punch}}. \tag{2.1}$$

As stated by Harpell (2000), "The LDR predictions were found to be sensitive to die radius changes but were less sensitive to the effect of changes in punch radius". This conclusion seems to be in accordance with the work of Simões (2012), which indicates that the deep drawing process is less sensitive to changes on the amount of lubricant applied to the punch. Also, a higher value of drawing ratio leads to a higher radial tension on the flange area and higher tensile stress is applied on cup's wall.

Lastly, one major problem in the deep drawing process is the influence of the anisotropy in the final results. The wall of a cylindrical cup, after the deep drawing process, has a non-equal high through the circumferential direction, called ears. This means that the anisotropy coefficient and the yield stress changes with the angle (α) to the rolling direction (RD), leading to different cup's high dependent on their distribution. The coefficient of plastic anisotropy (or *r*-value) is given by r_α, which is defined by:

$$r_\alpha = \frac{\bar{\varepsilon}_{yy}{}^p}{-(\bar{\varepsilon}_{xx}{}^p + \bar{\varepsilon}_{yy}{}^p)}. \quad (2.2)$$

The value of r_α is found through the analysis of tensile tests results, where $\bar{\varepsilon}_{xx}{}^p$ and $\bar{\varepsilon}_{yy}{}^p$ are, respectively, the average plastic deformations through the longitudinal and transversal direction to the direction of the applied load [Coër, 2013]. To have an accurate prediction of the ears at the end of the cup it is very important to know the anisotropic behaviour of the material. The sensibility of this phenomenon is usually represented by the planar anisotropy coefficient, Δr, which is given by:

$$\Delta r = \frac{r_0 + r_{90} - 2r_{45}}{2}, \quad (2.3)$$

where r_0, r_{45} and r_{90} are the values of the coefficients of plastic anisotropy through the three directions, 0º, 45º and 90º to RD, respectively. Finally, the tendency for earing is lower when the value of the planar anisotropy coefficient gets close to zero.

3. EXPERIMENTAL ANALYSIS

This chapter presents the details regarding the experimental analysis performed during this work. The first section is about the analysis of the tensile tests for the materials, 6061-T6 and 6016-T4 alloys, in order to evaluate their mechanical properties. After that, the results concerning the cup forming, including the description of the device are presented. The sheets (theoretically with a thickness of 1 mm) had been previously cold rolled, solution treated, quenched and naturally aged (T4 temper). T6 temper was made directly from T4 by heating T4 material at 150ºC for four hours followed by 170ºC for four hours in oil bath and subsequently quenched in water. The chemical compositions of the alloys are given in table 1. The 6016-T4 was furnished by Constellium France and the 6061-T6 by ULM technology in France but we don't know exactly its composition.

Table 3.1 – *r*, Δr and yield stress values for 6016-T4 at 200ºC.

Alloy	Si	Fe	Cu	Mn	Mg	Cr	Other
6016	0.9	0.25	0.1	0.17	0.413	0.039	<0.15
6061	0.4-0.8	Max 0.7	0.15-0.4	Max 0.15	0.8-1.2	0.05-0.35	<0.15

3.1. Tensile tests

In order to understand the behaviour of each material in the deep drawing process, several tensile tests (performed by V. Simoes during his PhD) were analysed at different temperatures, for 0º, 45º and 90º to RD in using a Gleeble machine. Figure 3.1 shows the results of the tests performed, for the 6016-T4 alloy. Concerning the yield stress, there are no significant differences between RT, 100ªC and 150ªC, and it decreases a little for 200ªC, having the temperature a low influence on this parameter. The hardening of each curve for different temperatures changes, being the highest value for RT and the lower one for 200ºC. Also, there is a decrease of the value of yield strength with the increase of temperature. Lastly, the yield stress and the hardening are only slightly affected by the direction of the tensile test.

In order to evaluate the anisotropy coefficients and the yield stress values, the elastic part of the tensile curves was removed. By convention, the yield stress value is

defined for 0.2% of strain. However, taking into account the flow stress evolution, it was decided to use as reference a value of 0.15%, for the 6016-T4 alloy. The *r*-values were estimated based on the linear trend for a plastic strain range between 0-10%. Table 3.2 and Table 3.3 presents the anisotropy coefficients and the yield stress values for the tensile tests performed, at RT and 200ºC, respectively. Despite the range of values for the yield stress, the trend is similar for both temperatures. This also occurs for the anisotropy coefficients, being the differences within the margin of error associated with their evaluation. As expected, the yield stresses at RT presents slightly higher values. Regarding the Δr values, as the 6016-T4 alloy at RT has the lowest value it is expect that it will present lower ears, as stated in the previous chapter.

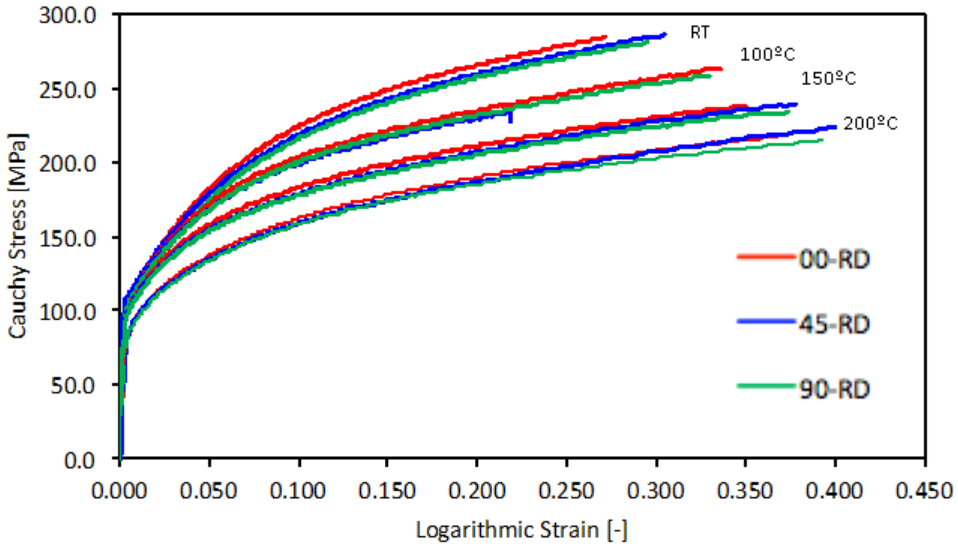

Figure 3.1 – True stress-strain curves for the 6016-T4 alloy.

Table 3.2 – *r*, Δr and yield stress values for 6016-T4 at RT.

α (º)	*r*-values	yield stress (MPa)
0	0.6558	104.608
45	0.5861	105.306
90	0.6243	106.357
Δr	0.054	

Table 3.3 – *r*, Δr and yield stress values for 6016-T4 at 200ºC.

α (º)	*r*-values	yield stress (MPa)
0	0.6927	91.136
45	0.6183	91.523
90	0.6681	91.863
Δr	0.062	

Concerning the 6061-T6 alloy, the same tensile tests were performed, and the results are presented in Figure 3.2. The stress-strain curves for RT, 100ºC and 150ºC have a similar hardening behaviour. Also, all present different values of the yield stress, i.e. a different behaviour than the 6016-T4 alloy. Finally, the stress-strain curves are quite similar for the three orientations tested, indicating a strong isotropic behaviour, for all temperatures.

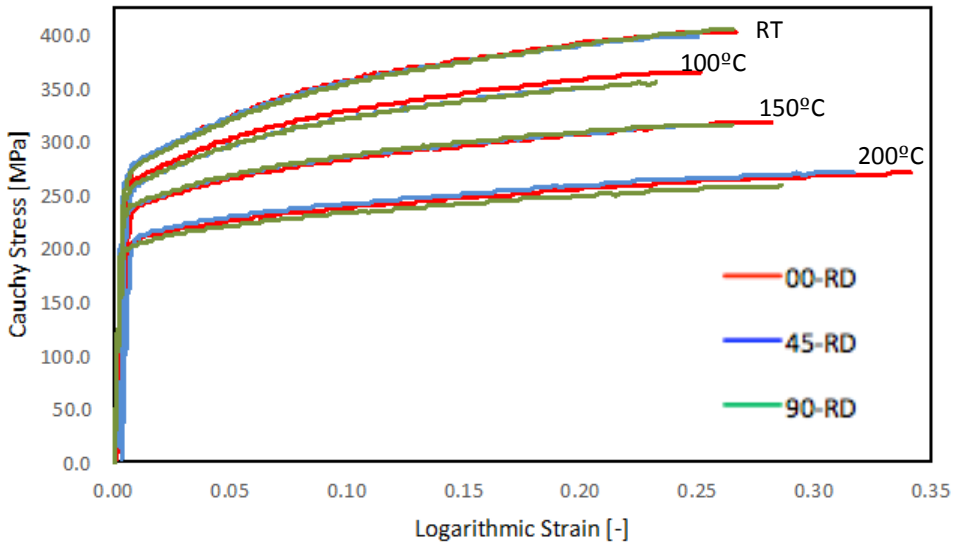

Figure 3.2 – True stress-strain curves for the 6061-T6 alloy.

The evaluation of the *r*-values was performed similarly to the 6016-T4 alloy. However, for the evaluation of the yield stress the reference strain values selected were 0.4% for RT and 0.35% for 200ºC. The determined values are presented in Table 3.4 for RT and Table 3.5 for 200ºC. The higher value for the anisotropy coefficient occurs at 0º, and the lowest for 90º, being the yield stress values almost constant, for both temperatures. The Δr values are quite similar for both temperatures, being slightly lower for 200ºC.

Table 3.4 – *r*, Δr and yield stress values for 6061-T6 at RT.

α (º)	*r*-values	yield stress (MPa)
0	0.706	279.191
45	0.5541	279.699
90	0.5465	279.503
Δr	0.072	

Table 3.5 – *r*, Δr and yield stress values for 6061-T6 at 200ºC.

α (º)	*r*-values	yield stress (MPa)
0	0.6863	213.051
45	0.6021	213.138
90	0.5427	213.124
Δr	0.012	

Both alloys present r_α values lower than one, indicating that the materials have a higher tendency to present deformation through thickness than width (see Equation (2.2)).

3.2. Results of cup forming

This section summarizes all the data collected from the experimental deep drawing tests performed. First the description of the device is detailed, explaining the tools used and their geometry, the thermocouples and all the factors relevant for the experimental analysis. Afterwards, details concerning the analysis of the data collected, including punch force and thickness evolution, is presented, considering the influence of temperature. The tests were performed for RT and 200ºC. The springback was also evaluated using the slit-ring test and the results are discussed. For each alloy and temperature, six experimental tests were performed. However, in this section only one experimental result is presented, considered as a reference for all, due to the fact that presents an average punch force evolution and an accurate initial temperature for the blank of 200ºC, in the case of warm tests.

3.2.1. Deep drawing device

The experimental procedure was performed in a Zwick/Roell-BUP200 machine as presented in Figure 3.3. The controlled parameters are the drawing speed, the blank-

holder force and the maximum punch displacement. In order to be able to compare results of this work with previous ones obtained for a 5xxx series alloy [Coër, 2013], the same experimental conditions were used, i.e. a blank-holder force of 6kN and a deep drawing speed of 1mm/s, both at room temperature and 200ºC. The gap between the punch and the die is 1.15mm, which will result in an ironing stage after the blank loss of contact with the blank-holder. In this work, the study of the lubricant amount was not a concern. Thus, all tests were performed considering a uniform amount of lubricant, trying to keep it as constant as possible, in order to obtain similar conditions between all tests.

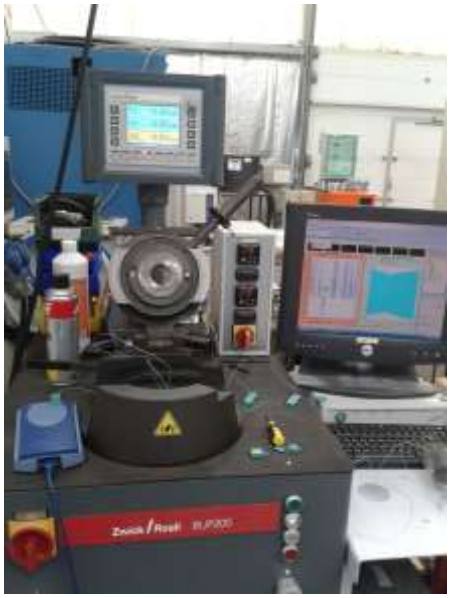

Figure 3.3 – Zwick/roell-BUP200 device and the acquisition system.

In order to control the temperature of the blank, thermocouples of type K were used. These thermocouples have a range of temperature between -200ºC to 1250ºC, with a limit of error of 0.75% above 0ºC (ANNEX A). The thermocouples were welded to the blank by arc welding (see Figure 3.4-(a)), one in the centre of the blank and the other at the limit of the punch radius, at 10 mm from the centre as present in Figure 3.4-(b). In order to be able to accurately measure the thickness evolution along the cup, this thermocouple is welded in a direction that is not aligned with 0º, 45º or 90º to the RD. As aluminium cannot be directly welded, first the blanks were sandblasted using the ARENA machine, presented in Figure 3.5.

(a)

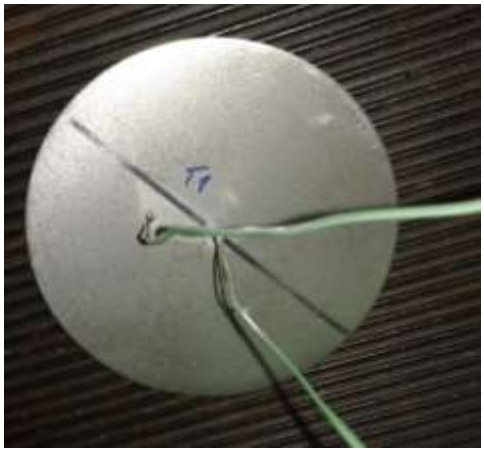

(b)

Figure 3.4 – (a) Arc welding machine; (b) Blank with the welded thermocouples.

Figure 3.5 – ARENA sandblast machine.

The tests performed at 200ºC, considered a blank-holder and die warmed until 200ºC, while the punch was cooled through air, trying to minimize its temperature. This conditions were selected following previous studies that shown that a combination of a warm die and a cold punch can reduce the amount of springback up to 20%, when compared to a conventional room temperature bending test [Moon et al., 2003]. The data concerning the temperature range in each tool and blank, and the punch force evolution was collected during all tests.

3.2.2. Influence of temperature in punch force

In this section the data regarding the punch force evolution with the drawing depth, during the cup forming is presented, for the two tests performed: one at room temperature and another one at 200ºC.

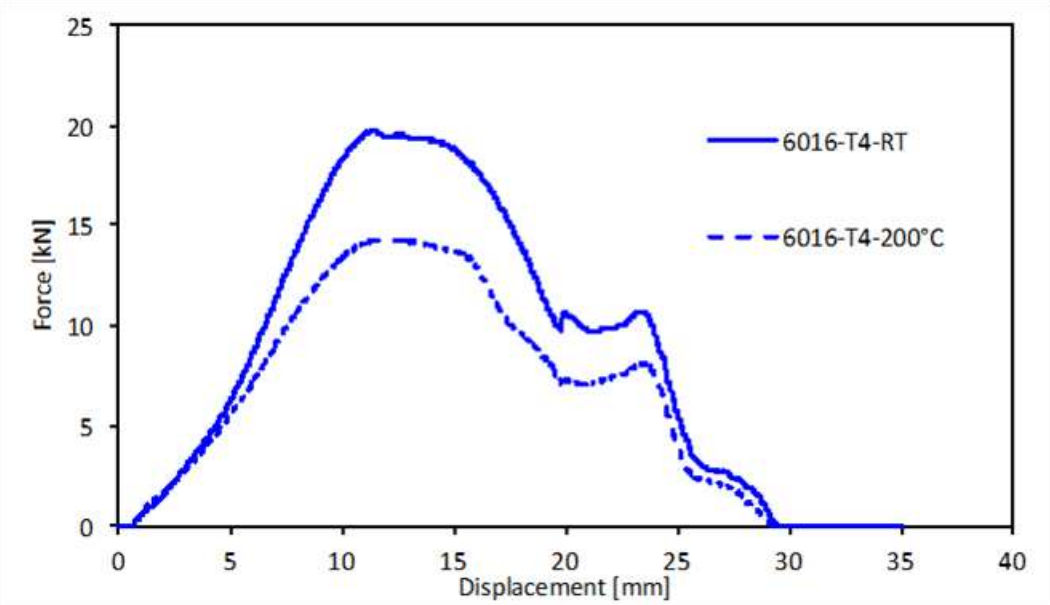

Figure 3.6 - Punch force evolution with the punch displacement for room temperature and 200ºC for 6016-T4.

Figure 3.6 presents the punch force evolution with the drawing depth for the 6016-T4 alloy, for both temperatures. Globally, the punch force decreases with the increase of temperature. The trend is similar for both tests in the drawing phase. However, after the 25mm displacement, when the ironing of the ears starts to occur, the curves present almost the same values. Table 3.6 presents the maximum force values as well as the absolute and percentage reduction for this alloy. The percentage of reduction of the punch force is quite similar for both the drawing and the ironing stages.

Table 3.6 – 6016-T4 Force reduction.

Temperature [ºC]	25	200
Max punch force in deep drawing [kN]	19.72	14.31
Reduction [kN]	-	5.31
Reduction	-	27%
Max punch force in ironing phase [kN]	10.73	8.12
Reduction [kN]	-	2.60
Reduction	-	24%

Figure 3.7 presents the results obtained for the 6061-T6 alloy, regarding the punch force evolution at room temperature and 200ºC. As for the 6016-T4, the punch force decreases with the temperature increase. Globally, both curves present a similar trend, with a drawing and an ironing phase occurring for similar values of drawing depth. Table 3.7 summarizes the reduction values, absolute and in percentage, concerning this alloy for both temperatures. The reduction for both maximum punch force values, in deep drawing and in ironing phase, is above 30%. In this case, a higher value of reduction was reached in the ironing phase.

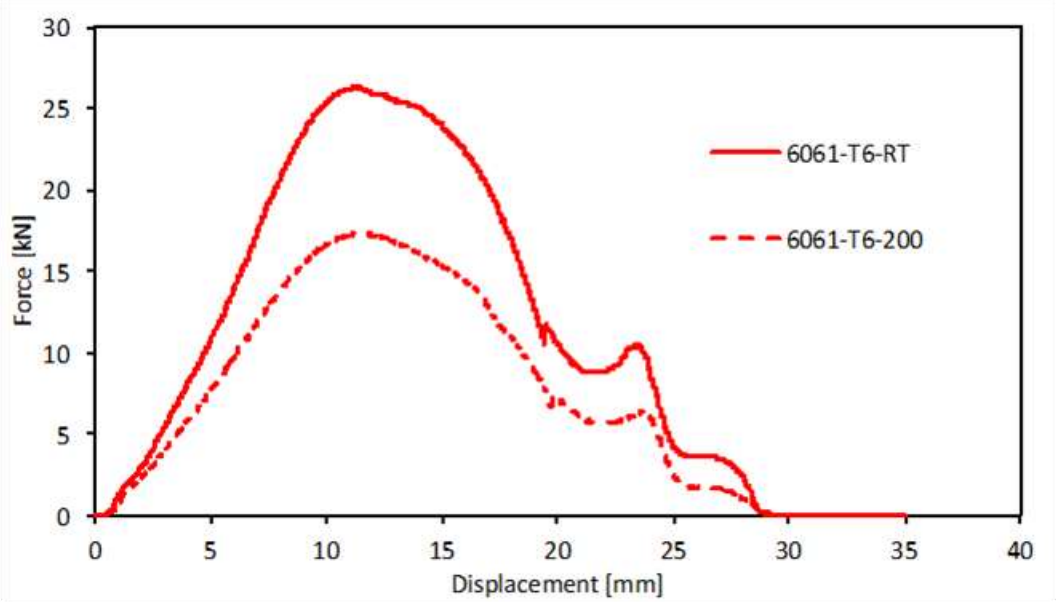

Figure 3.7 – Punch force evolution with the punch displacement for room temperature and 200ºC for 6061-T6.

Table 3.7 – 6061-T6 Force reduction.

Temperature [ºC]	25	200
Max punch force in deep drawing [kN]	26.28	17.34
Reduction [kN]	-	8.94
Reduction	-	34%
Max punch force in ironing phase [kN]	10.42	6.37
Reduction[kN]	-	4.06
Reduction	-	39%

3.2.3. Influence of temperature in thickness

The thickness is one of the most important parameters to measure after the cup forming. As stated by Gosh et al. (2012), the behaviour of the thickness is not regular along the cup. As presented in Figure 3.8, there are several zones that can be identified based on the thickness evolution along the cup's wall, which are detailed in the figure caption.

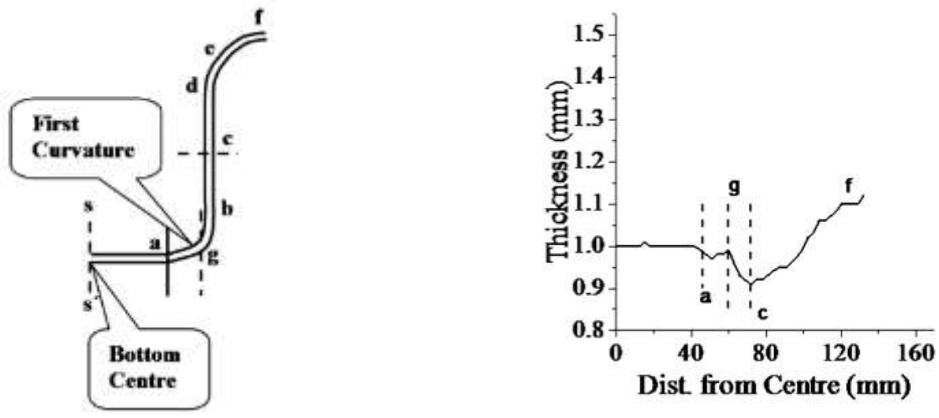

(a) (b)

Figure 3.8 - a) Schematic drawing of half the cross-section of a cup with the position of the different sections; sa: cup bottom; ss': punch axisymmetry axis; ab: zone around the punch radius; bd: cup wall; d: die throat; e: die profile radius; f: flange. (b) Thickness profile plot [Gosh et al., 2012]

Figure 3.9 – Brown & Sharpe machine to measure the thicknesses.

To perform the measures on each cup, the Brown & Sharp machine presented on Figure 3.9 was used. The procedure consists in fixing the cup on a vertical platform, and after that, with a program developed by Coër (2013), the needle measures the points on the inside and outside of the cup. After having the coordinates of all the points, along the 0º, 45º, 90º, 135º, 180º, 225º, 270º, 335º, the results are treated, to obtain the thickness along the cup. Since the cup is not exactly axisymmetric, an average through all the equivalent directions was performed.

Figure 3.10 presents the results for 6016-T4 alloy. To better understand these results it should be mentioned that the initial thickness of the blank was, in average 1.045mm. The thickness value for 200ºC is globally higher, which is in agreement with previous works done for the 5754-O alloy [Coër, 2012]. As the material as a lower hardening for 200ºC, this seems to contribute globally higher thickness values. The maximum thickness value is imposed by the ironing stage, being approximately 1.15mm. In this case, there is no strong thickness variation at the end of the cup's wall, indicating that the blank was not strongly retained by the blank-holder.

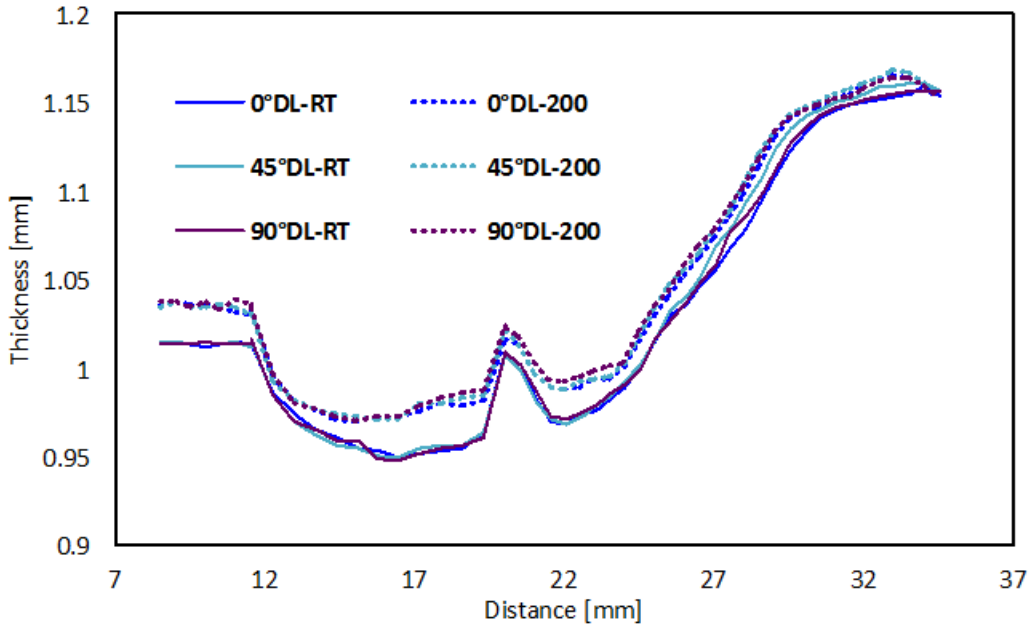

Figure 3.10 – Thickness evolution along the cup's wall for the 6016-T4 alloy to RT and 200ºC, in the three directions: 0º;45º;90º.

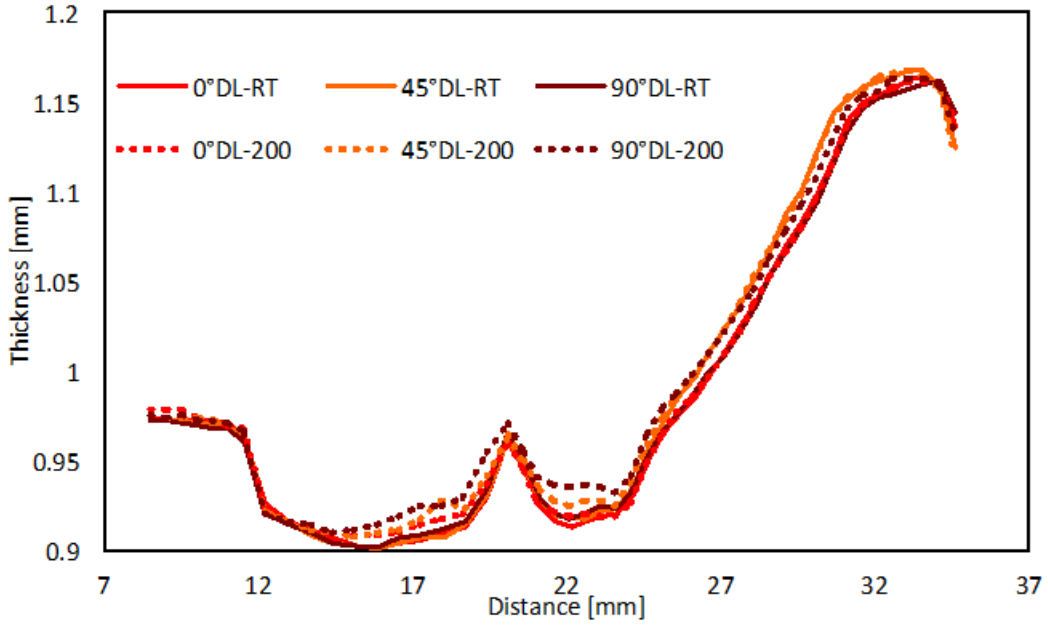

Figure 3.11 – Thickness evolution along the cup's wall for the 6061-T6 alloy to RT and 200ºC, in the three directions: 0º;45º;90º.

Figure 3.11 presents the results for 6061-T6 alloy, regarding the influence of temperature in thickness. Since the yield stress values of this alloy, at 200ºC, are still higher than the ones for 6016-T4 at RT, the blank holder presents a lower influence. Thus, this alloy seems flow more easily that the 6016-T4, reducing the temperature effect in the

thickness distribution. In this case, the cup's top suffers a significant decrease of thickness when compared to the 6016-T4 alloy.

Regarding the ears geometry, the measurement procedure was similar to the one used for the thickness. The machine performs a profile of the ears, by using a contact sensor, giving the coordinates of the cup's top. Four measurements were performed for each alloy, two at RT and two at 200ºC.

Concerning the 6016-T4, the influence of temperature on the ears geometry is presented on Figure 3.12. In this case, a higher temperature creates a lower cup, which may be related with the lower hardening for 200ºC. Regarding the anisotropy, since for both temperatures the material presents a Δr value higher than 0, the troughs occur for 45º to the RD, being the trend quite similar for both temperatures.

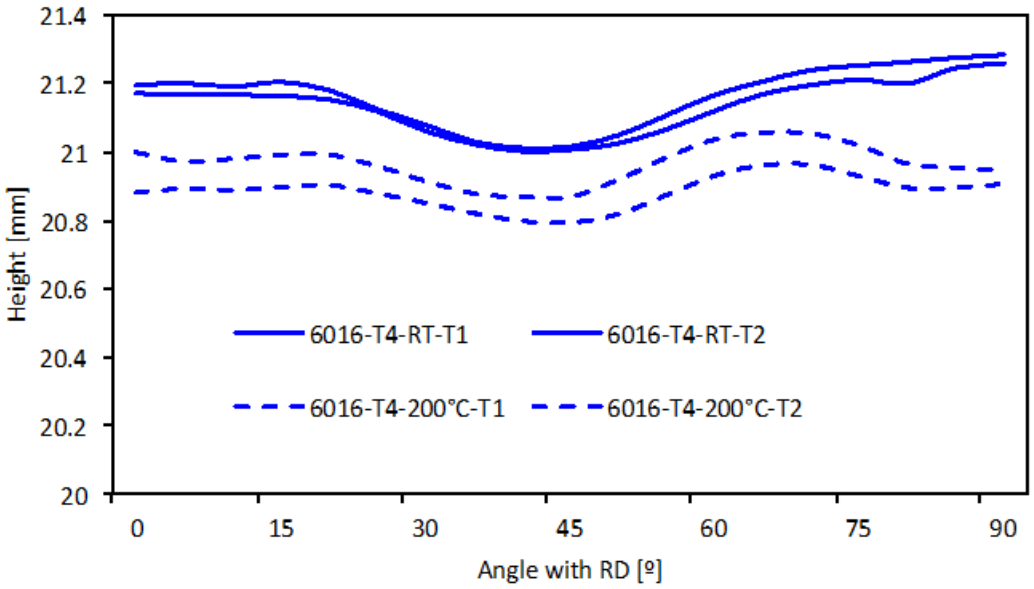

Figure 3.12 – Ears profile through the angle with the RD for the 6016-T4 alloy at RT and 200ºC.

Concerning the 6061-T6 alloy Figure 3.13 presents the results of ears variation with temperature. In this case, the temperature does not seems to influence the cup's height, which can be related with the stretching imposed by the blank-holder. Also, the troughs occur at 45º to RD, since the Δr values are higher than 0.

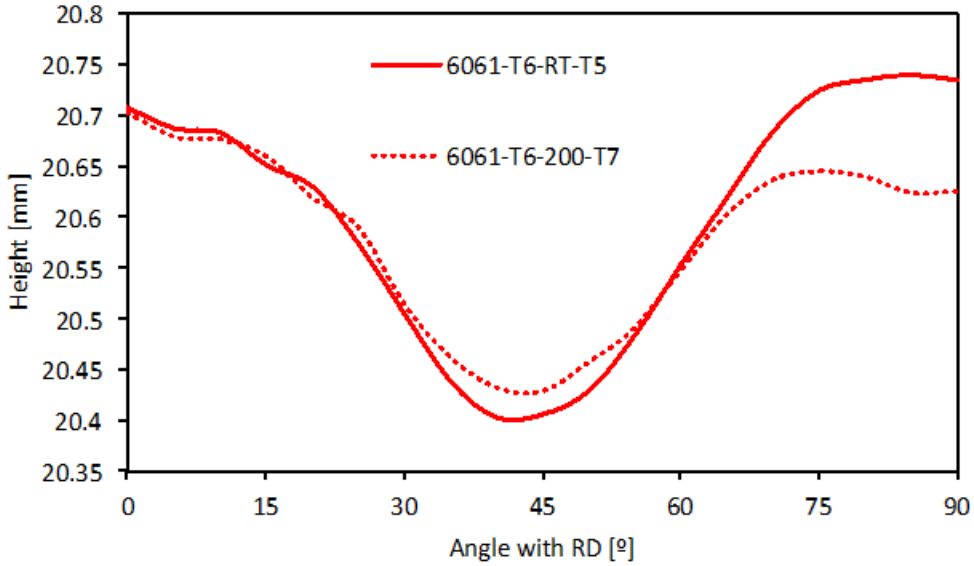

Figure 3.13 – Ears profile through the angle with the RD for the 6061-T6 alloy at RT and 200ºC.

The tests were performed with the same blank-holder force for the different alloys and different temperatures, for which the yield stress are different. Thus, the influence of the blank-holder is higher for the 6016-T4 alloy, with lower yield stress value than the one for 6061-T6, leading to lower cups for the later. Since the Δr values are very close to 0, the earing profile is quite smooth, i.e. the cup's height is almost isotropic.

3.2.4. Influence of temperature in Springback phenomenon

Springback was measured performing the Demeri test. As described in Figure 3.14, this test consists in three major steps: i) cut a slice at 8mm from the bottom; ii) cut a slice at 15mm from the bottom; iii) cut and measure the ring. With this, the ring will have a height of 7mm.

After the ring was cut, the measurement was made through a microscope to guarantee a high value of precision. Figure 3.15 shows an example of one of the measurements performed for both alloys. Each ring was measured twice, one facing upwards and the second facing downwards. The results presented correspond to an average of both results.

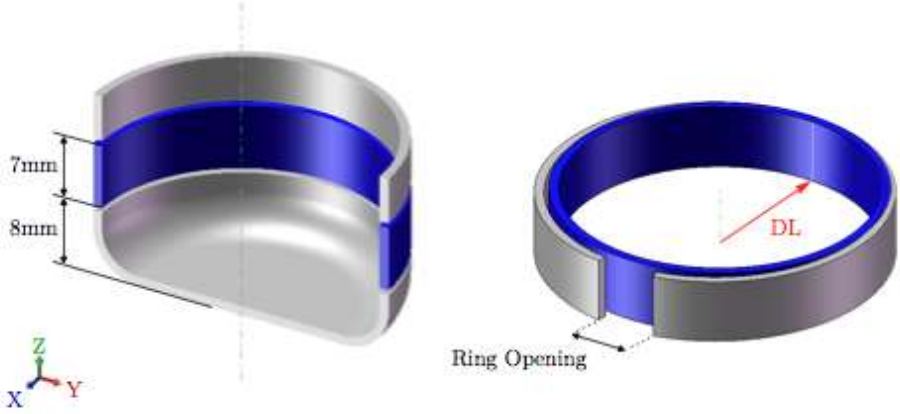

Figure 3.14 - Dimension of the ring and measurement of the overture after the springback [Coër, 2013].

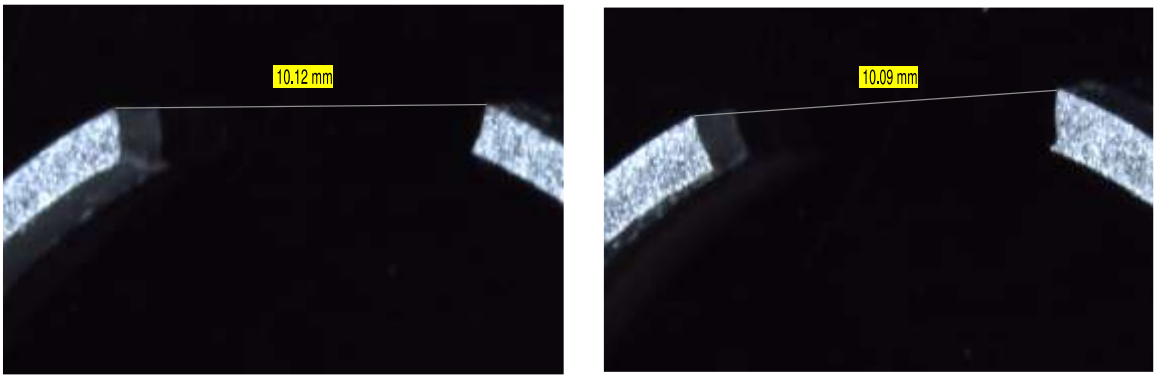

(a) (b)

Figure 3.15 – (a) Measurement of the springback facing upwards; (b) Measurement of the springback facing downwards.

Following the same order as the previous sections, the first measures presented are for the 6016-T4, including the absolute and percentage reduction achieved between the two temperatures (see Table 3.8). The reduction is quite similar to one previously reported by Moon et al. (2003) for 1050 alloy, considering the U-bent test.

Table 3.8 – 6016-T4 Springback measurements.

Temperature [ºC]	25	200
Averages [mm]	5.27	3.97
Reduction [mm]	-	1.30
Reduction	-	25%

For the 6061-T6 alloy, the springback results and the respective reductions are displayed in Table 3.9. A reduction of almost 50% was accomplished for the 200ºC test, when compared to the room temperature one.

Table 3.9 – 6061-T6 Springback measurements.

Temperature [ºC]	25	200
Average [mm]	10.10	5.69
Reduction [mm]	-	4.41
Reduction	-	44%

It is known that the springback increases with the decrease of the ratio between the yield stress and the Young modulus. It is also interesting to note that a lower reduction was found for the 6016-T4 alloy, corresponding to half of the value determined for 6061-T6. Since for the 6016-T4 the yield stress values are quite similar for both temperatures, the springback reduction seems to be mainly controlled by the small change in the Young modulus, which normally occur with the increase of temperature. On the other hand, for 6061-T6 the yield stress values decrease with the increase of temperature (~25%), which seems to contribute for increase in the springback reduction.

3.3. Comparison between 5754, 6016 and 6061

In this section a global comparison between the three alloys is presented. An analysis of the maximum punch force, for both phases, and also the springback was performed. All the values regarding the 5754-O alloy were taken from the work of Coër (2013).

Before presenting the comparison, Figure 3.16 presents the temperature evolution during the cups forming at 200ºC, for each tool, and both alloys, trying to highlight the trend observed during the test. The trend is similar for both alloys, although the 6016-T4 always presents the lowest values for all tools. Globally, the use of a cooled punch results in a temperature decrease of the blanks, during the test. It was for this reason that in section 3.1 the stress-strain curves were also presented for 150ºC.

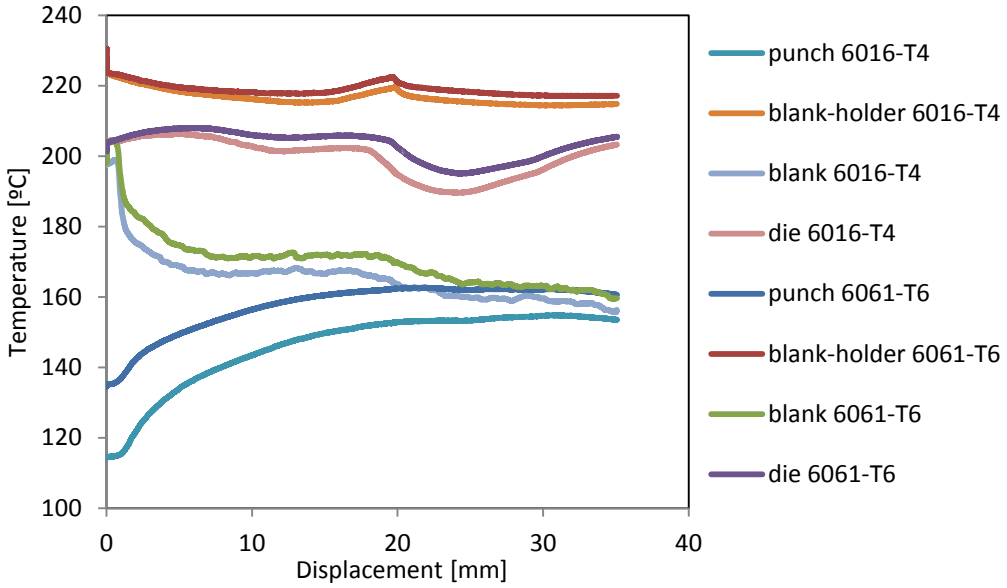

Figure 3.16 – Temperature evolution during the cup forming, for each tool, for both alloys, 6061-T6 and 6016-T4 at 200ºC.

Table 3.10 – 6061-T6 vs 6016-T4 vs 5754-O punch force and ironing reduction at RT.

Temperature [25ºC]	6061-T6	6016-T4	5754-O
Max punch force in deep drawing [kN]	26.28	19.72	17.30
Reduction [kN]	-	6.56	8.98
Reduction	-	25%	34%
Max punch force in ironing phase [kN]	10.42	10.73	9.70
Reduction [kN]	0.31	-	1.03
Reduction	3%	-	10%

Table 3.10 presents the comparison between the three alloys, 6016-T4, 6061-T6 and 5754-O, regarding the punch force during drawing and ironing reduction at RT. Concerning the maximum punch force for the deep drawing phase, the 6061-T6 has the highest value, which can be related with the higher strength. In fact, the reductions are much higher than for the ironing phase. For the ironing stage, the highest value occurs for the 6016-T4. In this stage high strain values are imposed to the sheet. However, the stress-strain curves presented in section 3.1 can only describe the hardening behaviour up to 30% of strain. The results indicate that 6016-T4 alloy presents higher hardening, which can be influencing the ironing force. Nevertheless, all alloys have similar values for this stage.

Table 3.11 – 6061-T6 vs 6016-T4 vs 5754-O punch force and ironing reduction at 200ºC.

Temperature [200ºC]	6061-T6	6016-T4	5754-O
Max punch force in deep drawing [kN]	17.34	14.31	13.50
Reduction [kN]	-	3.03	3.84
Reduction	-	17%	17%
Max punch force in ironing phase [kN]	6.37	8.12	5.50
Reduction [kN]	1.75	-	2.62
Reduction	22%	-	32%

The following comparison is for 200ºC, also for maximum punch force evolution and force in the ironing phase (see Table 3.11). Once again, 6061-T6 alloy achieves the highest value for maximum punch force in deep drawing, due to his higher strength, even though, the reduction is smaller, when compared to RT. For the ironing phase, 6016-T4 alloy has the highest value, as for RT. In fact, the temperature effect on the ironing force for this alloy is smaller when compared with the other alloys, which seems to indicate a different hardening behaviour also for 6016-T4 at 200ºC.

Figure 3.17 and Figure 3.18 are presented in order to compare the earing heights for the three alloys, for both temperatures. The results shows that the 5xxx series alloy presents a higher amplitude of the ears that the 6xxx series, which is in accordance to the values of planar anisotropy for the 5754-O, both at RT (Δr=-0.17) and 200ºC (Δr=-0.136), when compared with the ones of the 6016-T4 alloy, at RT (Δr=0.054) and 200ºC (Δr=0.062)) and of the 6061-T6 alloy, at RT (Δr=0.072) and 200ºC (Δr=0.012)) that are much closer to 0. Also, as the values of Δr for the 5xxx are negative, as shown in Figure 3.17, the toughs will occur at 0º and 90º, which is the opposite behaviour of the 6016-T4 and 6061-T6 alloys.

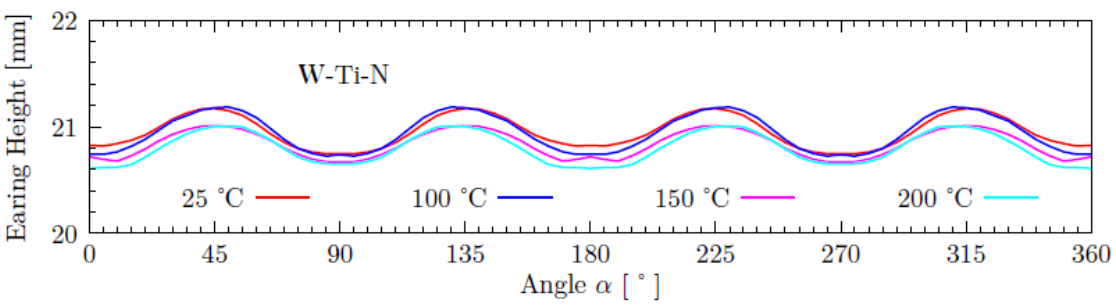

Figure 3.17 – Ears profile for the 5754-O at RT and 200ºC (extracted from Coër, 2013).

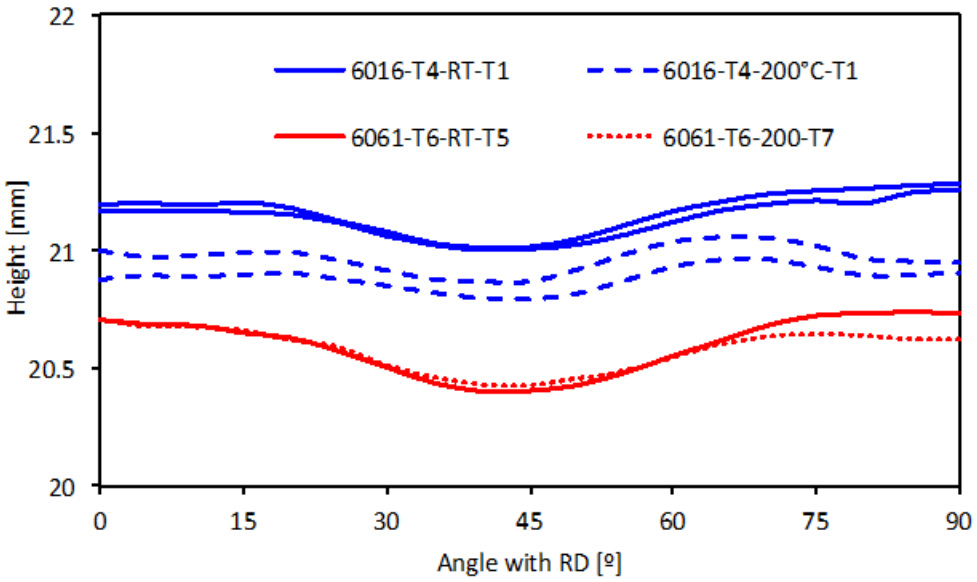

Figure 3.18 – Ears profile for the 6016-T4 and the 6061-T6 at RT and 200ºC.

The following results regard the springback analysis for the three alloys, although and analysis for the 6016-T4 and 6061-T6 was already made in section 3.2.4. The results are displayed in Table 3.12, for RT. 6061-T4 alloy achieves the highest value for the springback measurements, but also the biggest reduction (see Table 3.9), when compared with the other two alloys, which reach half the value of 6061-T6. Since the 5754-O and the 6016-T4 present comparable yield stress values, the reduction is quite similar. As previously mentioned, the ratio between yield stress and Young modulus seems to dictate the springback behaviour, i.e. 6061-T4 alloy presents the highest yield stresses for a similar Young modulus, therefore the highest value of springback.

Table 3.12 – 6061-T6 vs 6016-T4 vs 5754-O springback reduction at RT.

Temperature [25ºC]	6061-T6	6016-T4	5754-O
Average [mm]	10.10	5.27	5.87
Reduction [mm]	-	4.82	4.23
Reduction	-	48%	42%

Table 3.13 presents the results for 200ºC, concerning the three alloys. As 5754-O and 6016-T4 alloys have a similar yield stress at RT and at 200ºC, this reduction is caused mainly by the changing of the Young modulus with temperature. For the 6061-T6 alloy, it suffers a decrease of the yield stress from RT to 200ºC, reducing the difference

that occurred at RT to the other alloys, concerning the springback (see Table 3.9), reaching more similar values for 200ºC.

Table 3.13 – 6061-T6 vs 6016-T4 vs 5754-O springback reduction at 200ºC.

Temperature [200ºC]	6061-T6	6016-T4	5754-O
Average [mm]	5.69	3.97	4.67
Reduction [mm]	-	1.72	1.02
Reduction	-	30%	18%

4. NUMERICAL SIMULATION

The numerical simulation has a huge value to industries, predicting the behaviour and liability of a component, and quick adjusts to be made in order to optimize the process. Regarding the deep drawing process, the results studied were the punch force evolution, the thickness along the predefined directions (0º, 45º and 90º to RD) and the ears profile, at the end of the process. In order to be able to compare to previous studies, all numerical simulations were performed considering a die diameter of 35.30 mm, a blank-holder force of 6kN, isothermal conditions and an initial thickness blank of 1mm using the in-house code DD3IMP. Further details concerning the numerical model including the finite element type, blank discretization and tools modelling, can be consulted in Simões (2012).

Based on the information available for these aluminium alloys, 6061-T6 and 6016-T4, (i.e. yield stress and anisotropy coefficients for tensile tests performed along 0º, 45º and 90º to RD), it was decided to identify the anisotropy coefficients for both the Hill'48 and Barlat'91 (YLD'91). As referred by Habraken (1995), "The Hill (1948) criterion overestimates the differences in flow stress for aluminium alloys. The Barlat (1991) criterion performs better here." and also by Simões (2013), "the Hill'48 yield criterion is known by the inaccurate representation of materials with anisotropy coefficient < 1, as is the case of the aluminium alloys […]. The comparison between the numerical and the experimental results shows that better predictions are obtained with the YLD'91 criterion.".

Regarding the hardening law, two types of isotropic hardening laws are available in DD3IMP to describe the mechanical behaviour: The Swift law or the Voce law [Oliveira et al., 2007]. In this work, the saturation Voce law was selected to describe the classical isotropic work-hardening, which given by:

$$Y_f = Y_0 + (Y_{\boldsymbol{sat}} - Y_0)[1 - exp(-C_Y \bar{\varepsilon}^p)], \tag{4.1}$$

where Y_0, Y_{sat} and C_y are the material parameters and Y_f is the flow stress.

4.1. Material parameters identification

4.1.1. Hardening law

The identification was performed using the values of the tensile test presented in section 3.1, along the RD. The software used was either Gnuplot or Excel, which allow determining the best fit to the experimental values. The range for the equivalent plastic strain was always selected to perform the best fitting for higher values, since the deep drawing process attains strain values higher than 80%. The fitting was performed using the experiment data until an equivalent plastic strain of 25%. However, it should be mentioned that in the case of the 6061-T6 the maximum force in the tensile test occurs for 12% and 7%, for RT and 200ºC, respectively. For the 6016-T4 the value of 25% is a good approximation for both temperatures. In order to help the analysis of the hardening behaviour of the materials, although the Swift law was not used, the hardening coefficient, n is also reported for all materials.

Regarding the 6016-T4 alloy, Figure 4.1 gives the comparison between the stress-strain curve of the tensile test performed, red line, and the set of points that were adapted to the experimental values, green line.

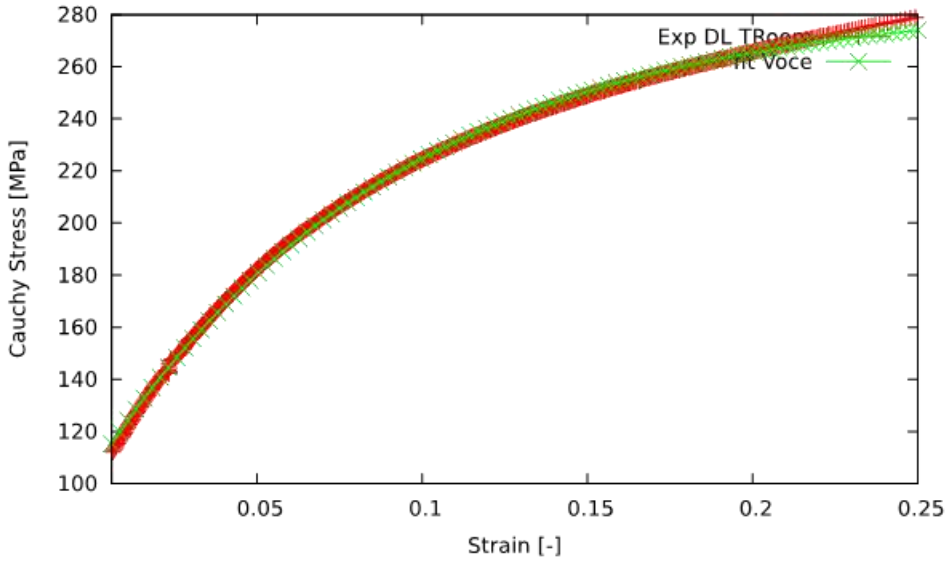

Figure 4.1 – Curve adjusted to tensile test through Gnuplot to 6016-T4 at RT.

A different method was used to determine the material parameters for 6016-T4 at 200ºC. The values of the experimental tensile curve were displayed on Excel and the Voce law was encoded as a function of the material parameters. An error function was

calculated between the numerical values and the experimental ones. The Solver application was used to minimize this error function, determining the best parameters. At 200ºC we have a higher value of Y_0 than the yield stress previously reported, as shown in Table 4.1, because more importance was given to the final part of the curve. Lastly, the parameters for the 6016-T4 alloy, at RT and 200ºC, are displayed in Table 4.1.

Table 4.1 – Final set of parameters to 6016-T4 at RT and 200ºC.

	Y_0	Y_{sat}	C_y	n
RT	103.772	285.751	10.9403	0.271
200ºC	105.9841	219.1686	7.2853	0.233

Figure 4.2 presents the comparison between the fitted hardening laws and the experimental data, for both temperatures. It is shown that the fact that the fitting was performed using the experiment data until an equivalent plastic strain of 25%, still leads to some differences in the final part of the curves. Anyhow, the n value, which dictates the hardening coefficient is higher for the RT, indicating a slightly higher hardening.

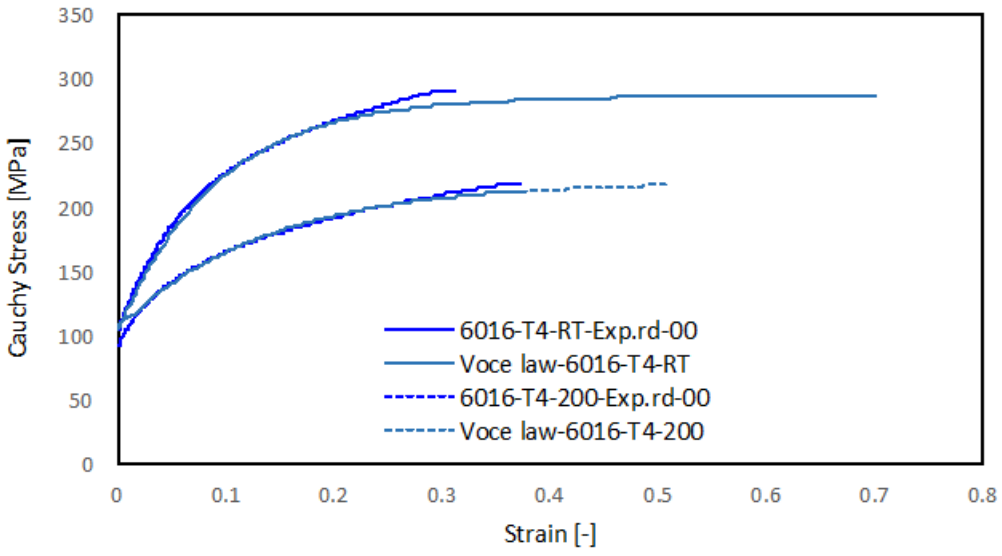

Figure 4.2 – Comparison between the experimental curve and the Voce law one to the 6016-T4 alloy at RT and 200ºC.

The same procedure was made to 6061-T6 using Gnuplot, for both temperatures. Figure 4.3 presents the hardening law determined for RT. Regarding the 200ºC, for the 6061-T6 alloy, Figure 4.4 presents the better adjustment made with Gnuplot.

Lastly, all the parameters obtained through the Gnuplot are displayed in Table 4.2 for a better comparison of the values.

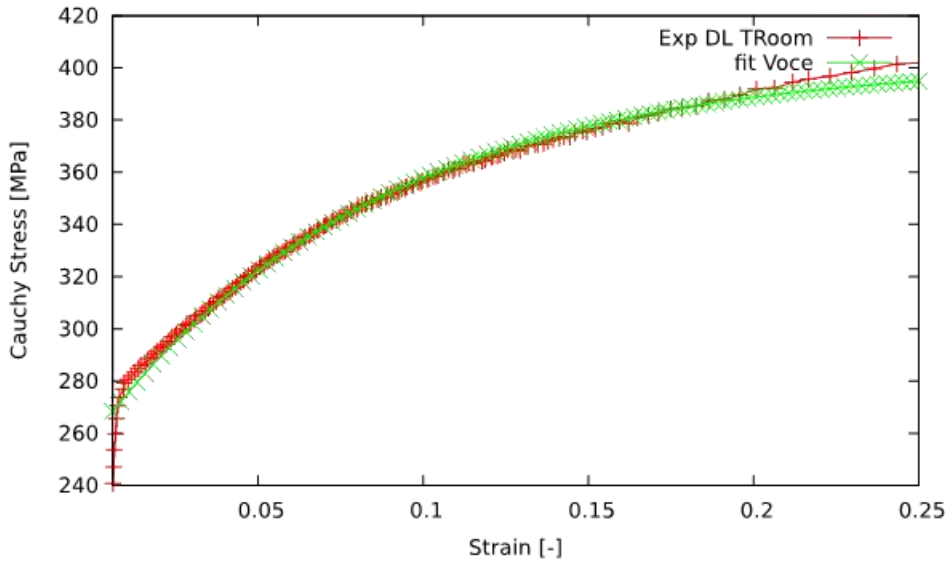

Figure 4.3 - Curve adjusted to tensile test through Gnuplot to 6061-T6 at RT.

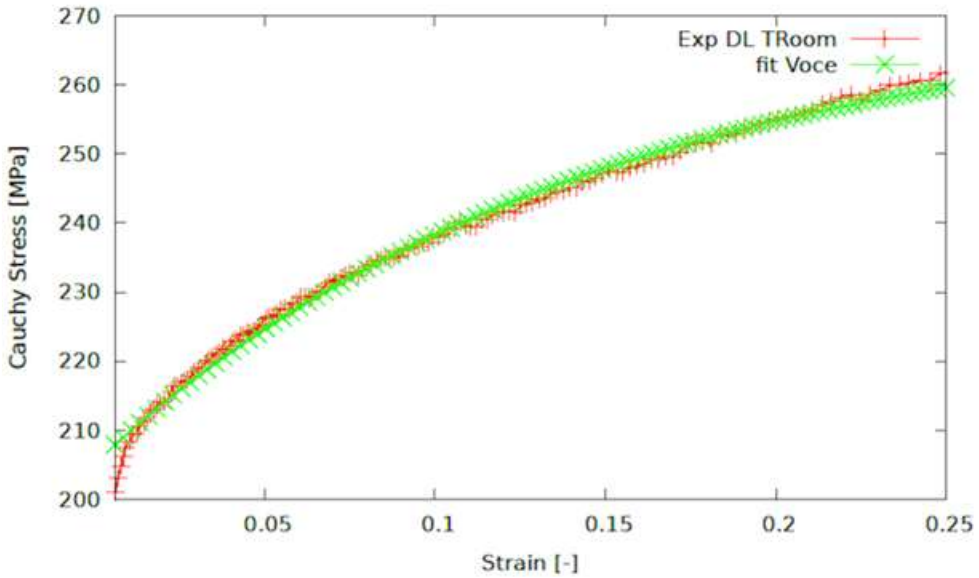

Figure 4.4 - Results obtained through Gnuplot to 6061-T6 at 200ºC.

Table 4.2 – Final set of parameters to 6061-T6 at RT and 200ºC.

	Y_0	Y_{sat}	C_y	n
RT	258.603	402.724	11.6558	0.127
200ºC	205.186	271.052	6.98989	0.085

The comparison between the fitted hardening laws and the experimental data is presented in Figure 4.5, for both temperatures. It is shown that the fact that the fitting was performed given more importance to the experiment data for higher equivalent plastic strain values, leads to some differences in the yield stress fitting (compare Table 3.4 and Table 3.5 with Table 4.2). The n value is higher for the RT, indicating a higher hardening. Also, although the C_y is quite similar for both alloys, for both temperatures, since the difference between Y_0 and Y_{sat} is higher for the 6016-T4 alloy, it can be stated that it presents a higher hardening, for both temperatures.

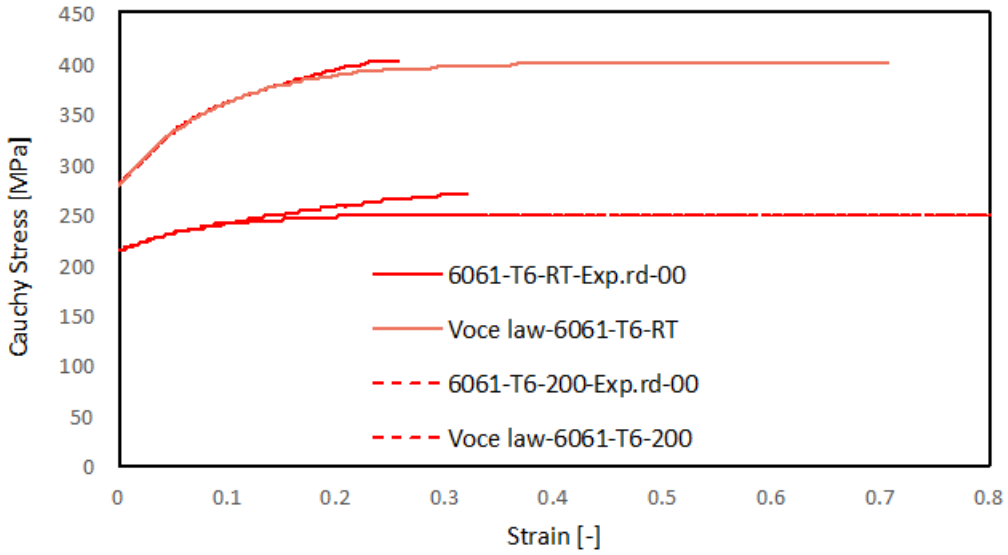

Figure 4.5 - Comparison between the experimental curve and the Voce law one to the 6061-T6 alloy at RT and 200ºC.

4.1.2. Yield criteria

The yield criteria were identified using the DD3MAT program, which is based on the minimization of the error between the experimental *r*-values and yield stress and the numerical ones. Thus, besides the experimental data previously presented in section 3.1, it is also necessary to define the elastic properties and the hardening law. The last was already summarized in the previous section. Regarding the elastic properties it was considered that the Poisson coefficient remains constant with temperature, being equal to 0.33. Previous results for the Young modulus, obtained for the 5754-O, indicate that it decreases with temperature. Thus, based on the experimental data available for that alloy it

was assumed that both 6000 series alloy present an Young modulus of 70 GPa at RT and 61 GPa at 200ºC, similarly to the 5754-O (Coër, 2013).

Table 4.3 and Table 4.4 displays the values obtained for 6016-T4 at RT and 200ºC, respectively, for the Hill'48 and Barlat'91 criterion (m=8).

Table 4.3 – Barlat'91 and Hill'48 parameters for 6016-T4 at RT.

Barlat'91 Parameters				
C1	C2	C3	C4=C5	C6
1.0572	1.0428	0.9444	1.0	0.9498
Hill 48 Parameters				
F	G	H	L=M	N
0.61007	0.5858	0.3821	1.5	1.3003

Table 4.4 – Barlat'91 and Hill'48 parameters for 6016-T4 at 200ºC.

Barlat'91 Parameters				
C1	C2	C3	C4=C5	C6
1.23315	1.21989	1.09634	1.0	1.12075
Hill 48 Parameters				
F	G	H	L=M	N
0.82163	0.795978	0.549564	1.5	1.810767

Figure 4.6 shows that both yield criteria fit quite accurately the *r*-values for both RT and 200ºC. However, for the yield stresses the same is not observed, being the differences between experimental and numerical results slightly higher for the Hill'48. Based on the experimental results, this material presents a slight anisotropic stress behaviour, which trend is not well described by the Hill'48 criterion. The yield surface in the plane $\sigma_1-\sigma_2$ is displayed in Figure 4.7, for both temperatures, where the von Mises is also included as a reference. Taking into account Figure 2.4, we can relate this graphic with the different parts of the cups, the centre, the wall and the flange. For RT, the behaviour of both criteria, Barlat'91 and Hill'48, is quite similar, excepted close to pure shear and in the biaxial point. Regarding the 200ºC, the results are quite similar to the ones obtained at RT, also with a better fit of the *r*-values than the yield stress. Regarding the yield surface in the $\sigma_1-\sigma_2$ plane it shows that the highest differences between both yield criteria occurs for the same stress states. The reason why von Mises surfaces for both temperatures are almost coincident, is related with the values of Y_0, which for this material,

are very similar at RT and 200ºC (see Table 4.1). Since this criterion does not considers the anisotropy of the material, it will only take into account the Y_0 value.

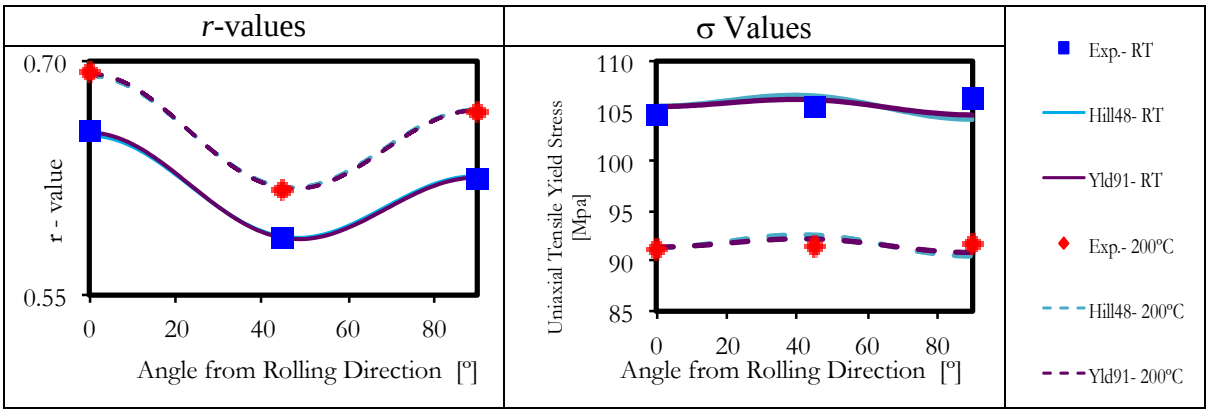

Figure 4.6 – Comparison between RT and 200ºC for the 6016-T4 alloy for: (a) *r*-Values; (b) yield values.

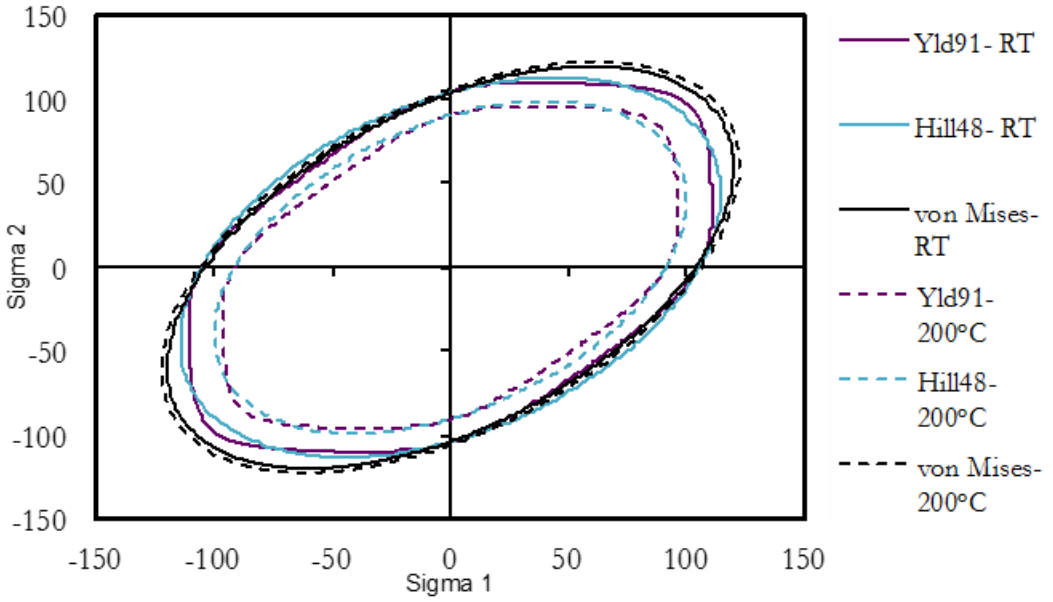

Figure 4.7 – Yield surface in the plane σ_1–σ_2 for the 6016-T4 at RT and 200ºC.

The same procedure was made for the 6061-T6 alloy at RT and 200ºC and the results are presented in Table 4.5 and Table 4.6, respectively. Figure 4.8 presents the evolution of the *r*-values and yield stresses in the sheet plan, which were once again used to build the σ_1–σ_2 surface, which is shown in Figure 4.9. In this case, the experimental yield stress values are quite isotropic, which cannot be accurately represented by both yield criteria. Regarding the *r*-values, they are accurately described by both yield criteria.

Regarding the $\sigma_1-\sigma_2$ surface, a difference is perceptible between the criteria at RT and 200ºC, due to the distinction of the Y_0 value for this alloy in both temperatures. Comparing both criteria, for each temperature, the yield surfaces of each are quite different between the plane strain until the pure shear.

Table 4.5 – Barlat'91 and Hill'48 parameters to 6061-T6 at RT

Barlat'91 Parameters				
C1	C2	C3	C4=C5	C6
1.03151	0.95346	0.8636	1.0	0.890135
Hill 48 Parameters				
F	G	H	L=M	N
0.60192	0.47619	0.33234	1.5	1.13749

Table 4.6 – Barlat'91 and Hill'48 parameters to 6061-T6 at 200ºC

Barlat'91 Parameters				
C1	C2	C3	C4=C5	C6
1.067795	0.51782	0.35185	1.0	0.937396
Hill 48 Parameters				
F	G	H	L=M	N
0.64143	0.51782	0.35185	1.5	1.27749

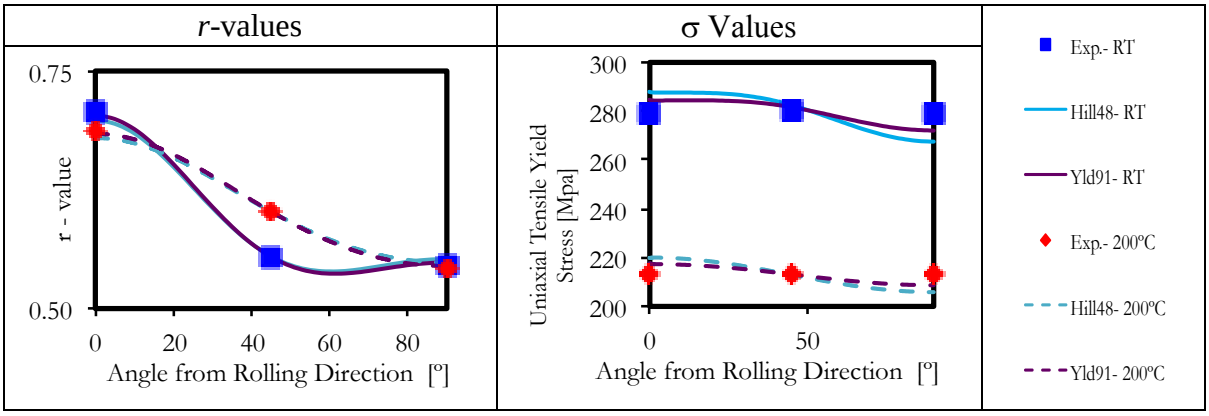

Figure 4.8 – Comparison between RT and 200ºC for the 6061-T6 alloy for: (a) *r*-Values; (b) yield values.

Globally, both yield criteria lead to similar results, since the main advantage of the Barlat'91 was not explored due to the lack of experimental data concerning the biaxial stress state. For the 6016-T4, for both temperatures the shape of the yield surface is quite similar, reflecting the similarities in the anisotropic behaviour. For the 6061-T6, the

differences in the yield surface shape are higher for both temperatures, since the experimental trend of the *r*-values is also more different.

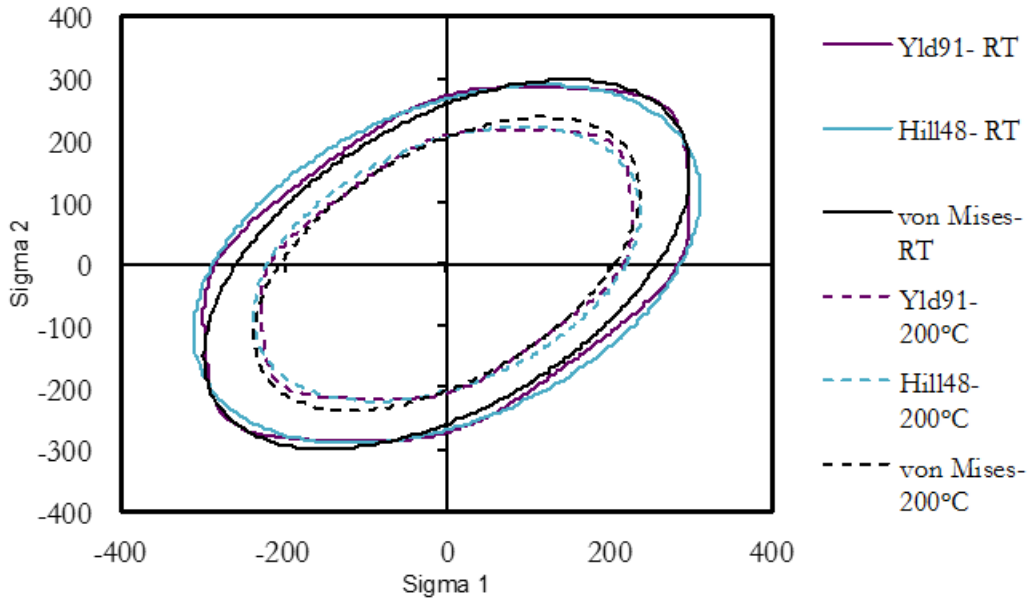

Figure 4.9 - Yield surface in the plane σ_1–σ_2 for the 6061-T6 at RT and 200ºC.

4.2. Flow conditions analysis

Previous works shown that the friction coefficient is very difficult to measure, since it is a local effect that is commonly modelled with a single constant values [Coër, 2013] and [Simões, 2012]. These studies also confirm that the friction coefficient affects both the deep drawing and the ironing stages. Thus, since the material flow is directly connect to the yield criteria and the friction coefficient, a trial and error approach was adopted in order to determine the best combination between both. The selection of the best result was performed using as reference the experimental punch force evolution with its displacement. This comparison is performed considering all the six experimental tests performed, to highlight the range of the tests. This section presents only the results obtained with the friction coefficient that better fits the experimental data, for each alloy and each temperature.

In order to try to understand which yield criteria better fits to the experimental results, an analysis of the stress states was performed based on the surfaces represented in the σ_1–σ_2 plane. The assumption is that the materials under analysis presents almost an

isotropic behaviour. Thus, another criteria for the selection was the better correlation with the von Mises one, for the stress states that occur in the cup (see Figure 2.4).

Figure 4.10 presents the punch force evolution with its displacement for the 6016-T4 alloy, at room temperature. A value of 0.15 for the friction coefficient fits quite well the first 12mm of displacement. Nevertheless, after this value, the punch force numerically predicted underestimates the experimental one. Also, the loss of contact with the blank-holder occurs later indicating that the material flows faster in the experimental test. The underestimation of the force also occurs for the ironing phase. The Hill'48 yield criterion fits better to the experimental results, during the first 12mm of punch displacement, but also in the ironing phase. The Hill'48 criterion its closer to von Mises for plane strain and uniaxial stress, while Barlat'91 is closer for shear state. Thus, this seems to contribute to a better prediction of the maximum punch force evolution with Hill'48.

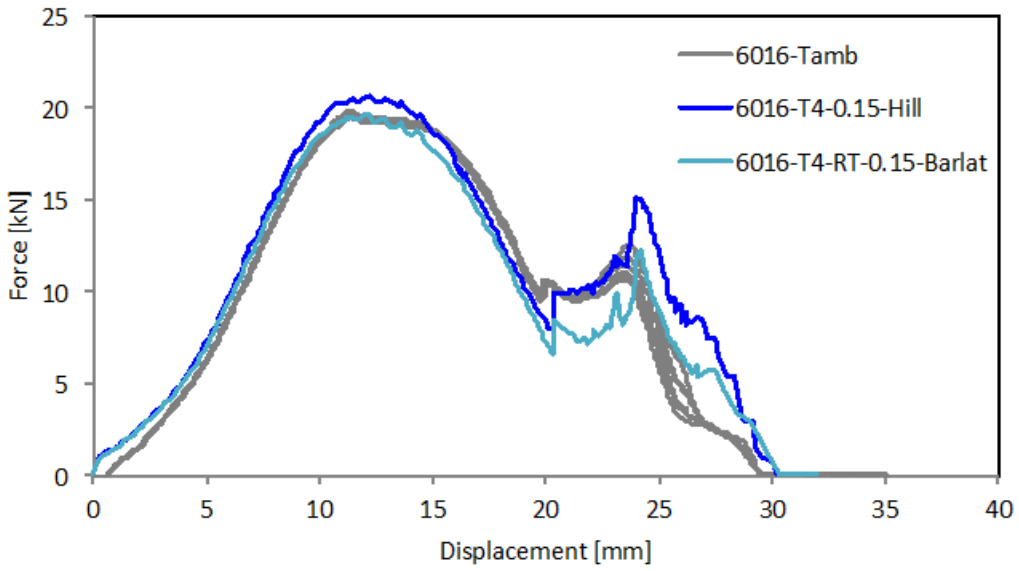

Figure 4.10 – Comparison of the punch force evolution with the punch displacement between experimental and numerical analysis for the 6016-T4 alloy at RT.

Figure 4.11 presents the results for the 6016-T4 alloy at 200ºC. In this case a value for the friction coefficient of 0.175 was the one that better fitted to the experimental curves. It should be mentioned that higher values of friction coefficient lead to necking, in the numerical simulations. In fact, the moment of contact loss between the blank and the blank-holder is overestimated in the numerical analysis, indicating that the material flow

slower. Thus, although there is globally an underestimation of the punch force it was decided to keep the value of 0.175, for the following analysis. The Hill'48 criterion adjusts better to von Mises, between plane strain and pure shear stress states (Figure 4.7). It better fits the maximum punch force in the drawing and the ironing phases.

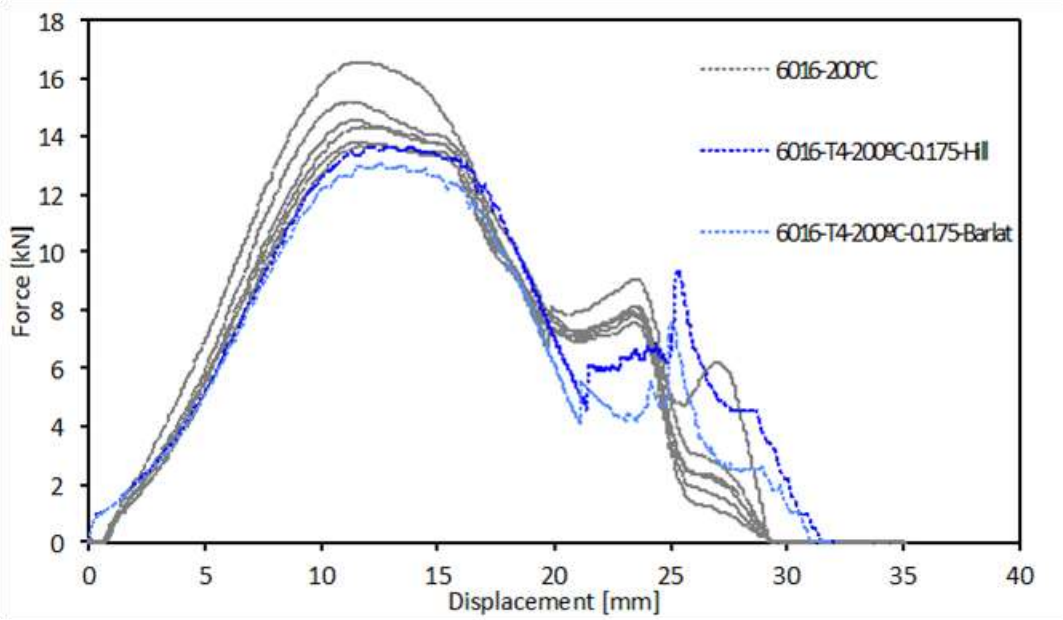

Figure 4.11 - Comparison of the punch force evolution with the punch displacement between experimental and numerical analysis for the 6016-T4 alloy at 200ºC.

The same procedure was made for the 6061-T6 alloy. As Figure 4.12 demonstrates, the value of the friction coefficient that better fit the experimental curves is 0.1, although, this value is only suitable until 18mm. An overestimation of the value for the ironing phase occurs. Taking the von Mises yield criterion as reference, Figure 4.9 shows that the Hill'48 spreads more than the Barlat'91 for plane strain and pure shear states. Thus, although there is an overestimation after the 20mm, the Barlat'91 criterion adjusts better to the experimental curves, being used to the following analysis.

Regarding the 200ºC, the friction coefficient that adjusts better the numerical simulations with experimental curves is also 0.10, as shown in Figure 4.13. Considering the von Mises as reference, the Hill'48 criterion is closer at the plane strain stress, while the Barlat'91 is closer for the pure shear. The criterion selected is the Barlat'91 with a friction coefficient of 0.10.

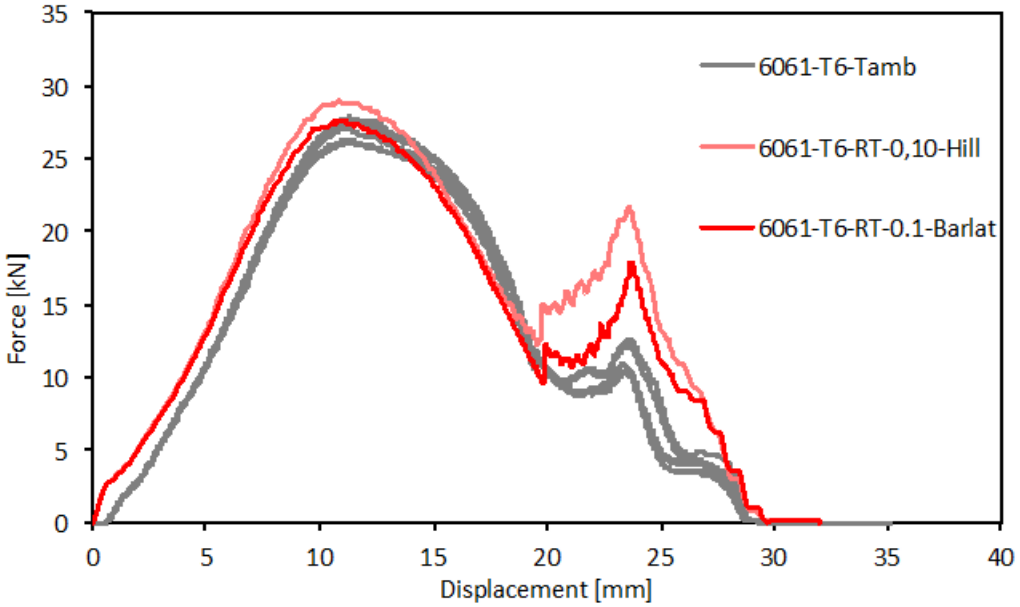

Figure 4.12 - Comparison of the punch force evolution with the punch displacement between experimental and numerical analysis for the 6061-T6 alloy at RT.

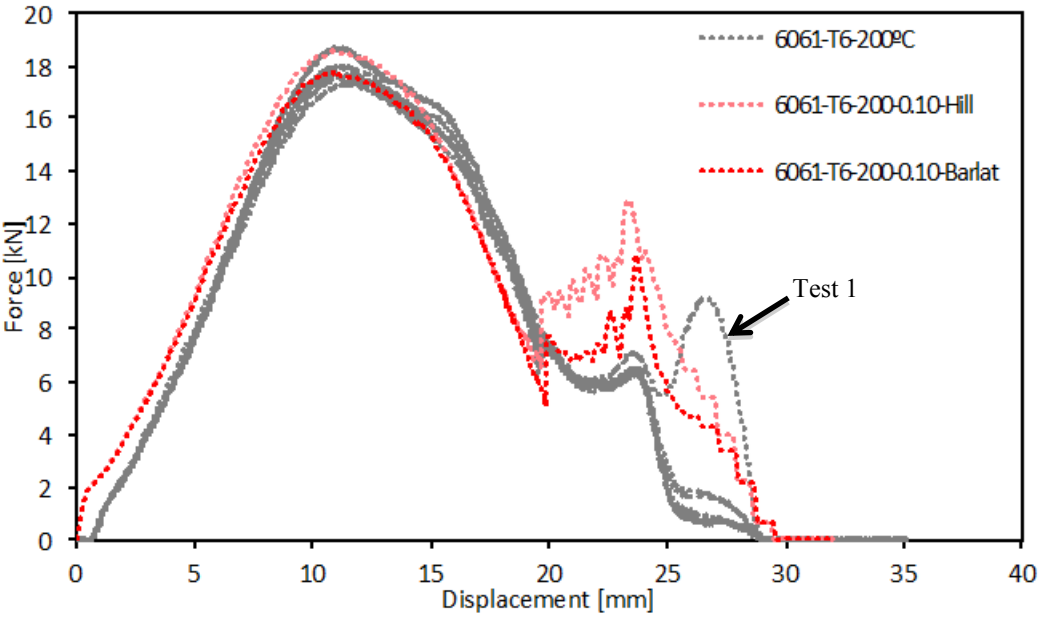

Figure 4.13 - Comparison of the punch force evolution with the punch displacement between experimental and numerical analysis for the 6061-T6 alloy at 200ºC.

4.3. Results of cup forming numerical simulations

In this chapter the results for the selected numerical simulations are shown, trying to understand the influence of temperature in three major factors: punch force; thickness evolution along the cup's wall; and ears profile.

4.3.1. Influence of temperature in punch force

The results are firstly presented for the 6016-T4 alloy, following the same strategy adopted in the previous sections. Figure 4.14 shows the results for the numerically predicted punch force evolution with its displacement, for both temperatures, RT and 200ºC. Three results are presented: one at RT, with a friction coefficient of 0.15, and the other two at 200ºC, one with a friction coefficient of 0.175, and the other with 0.15, to have a comparison with the same friction coefficient value at RT. The increase of the friction coefficient at 200ºC leads to a change in the material flow and, consequently, to a loss of contact between the blank and the blank-holder for a higher punch displacement.

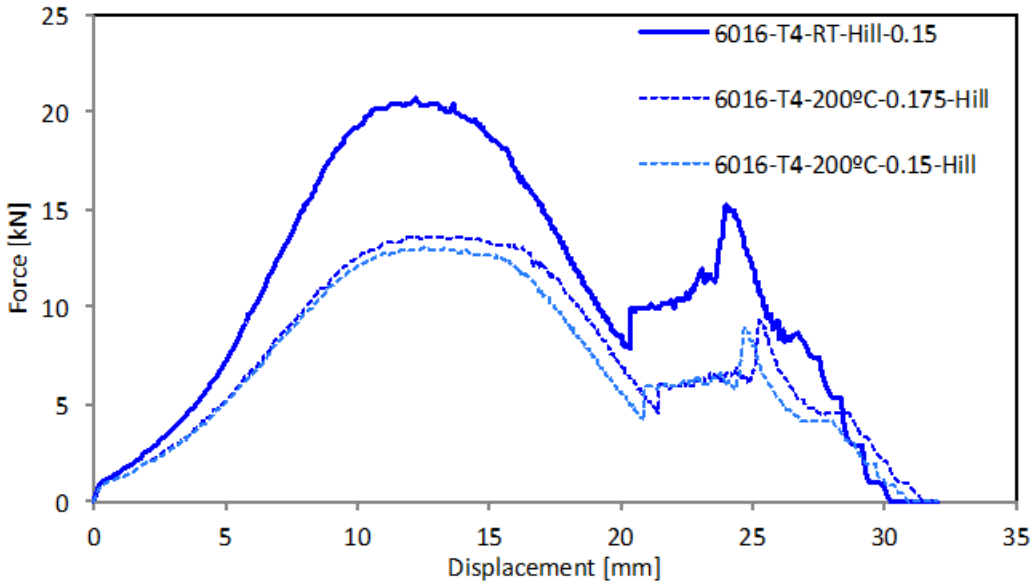

Figure 4.14 - Punch force evolution with the punch displacement for RT and 200ºC for the 6016-T4 alloy.

Table 4.7 presents the values of the force reduction due to the increase of temperature, for the 6016-T4 alloy. At RT the peak of force in the ironing phase is much higher when compared to 200ºC, originating the highest value of reduction.

Table 4.7 – 6016-T4 Force reduction in numerical analysis between RT and 200ºC.

Temperature [ºC]	25	200
Max punch force in deep drawing [kN]	20.58	13.67
Reduction [kN]	-	6.91
Reduction	-	34%
Max punch force in ironing phase [kN]	15.57	9.35
Reduction [kN]	-	6.22
Reduction	-	40%

Regarding the 6061-T6 alloy, the results are shown in Figure 4.15, and present a similar trend in the evolution of the force during the entire test, including the displacement for which the blank-holder loss contact with the blank. Regarding the amplitude of the force in the ironing phase, higher values are attained at RT due to higher maximum thickness values at the cup's top.

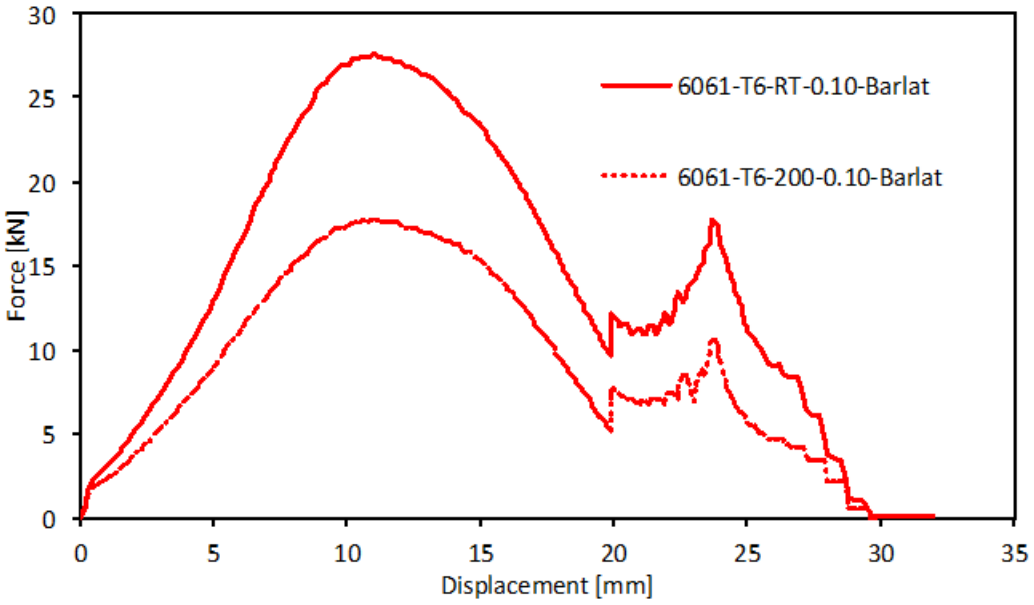

Figure 4.15 - Punch force evolution with the punch displacement for RT and 200ºC for the 6061-T6 alloy.

The values of the force reduction due to the temperature increase for the 6061-T6 alloy, are presented in Table 4.8. In this case, the reduction in both phases is quite similar, having the temperature an effect on the force values, but not in the curves trend. This seems to be related with the fact that for 200ºC the hardening is much lower than for

the RT. The same is not valid for the 6016-T4 alloy, which presents values more similar for both temperatures.

Table 4.8 – 6061-T6 Force reduction in numerical analysis between RT and 200ºC.

Temperature [ºC]	25	200
Max punch force in deep drawing [kN]	27.56	17.77
Reduction [kN]	-	6.97
Reduction	-	35%
Max punch force in ironing phase [kN]	17.77	10.8
Reduction [kN]	-	6.97
Reduction	-	39%

4.3.2. Influence of temperature in thickness

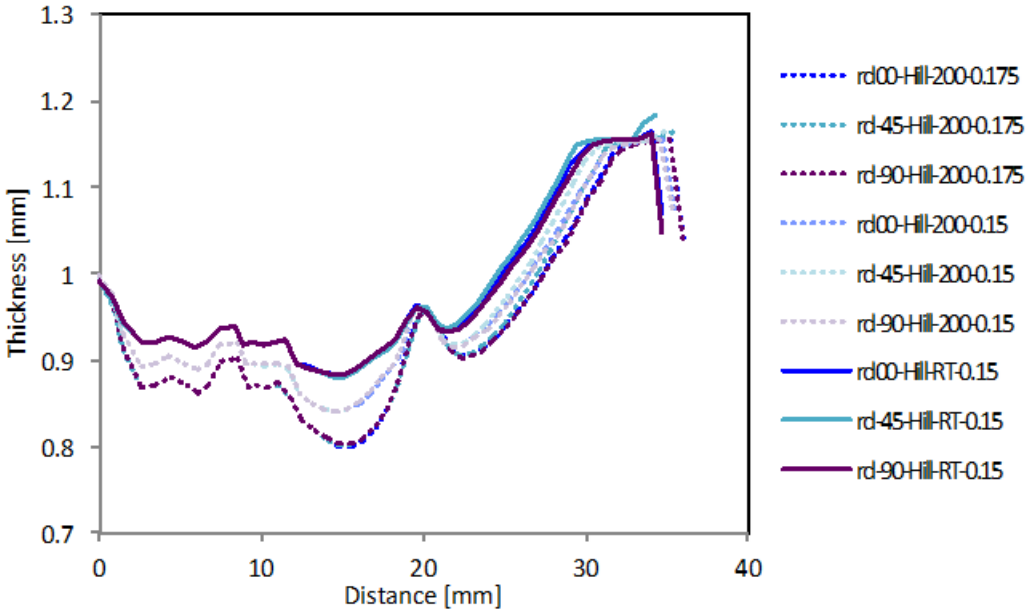

Figure 4.16 – Thickness evolution along the cup for RT and 200ºC for the 6016-T4 alloy.

The results for the 6016-T4 alloy are presented in Figure 4.16. A friction coefficient of 0.15 was used at RT, and one of 0.175 at 200ºC. However, in order to have a more precise comparison between numerical results, the prediction obtained with a value of 0.15 at 200ºC is also presented. It is noticeable that the 6016-T4 alloy suffers a strong thickness decrease in the cup's bottom, being this value influenced by the friction

coefficient. Also, the squeeze along TD suffered at both temperatures is almost the same, although slightly higher at 200ºC, as the material was more retained by the BH, originating a wall with lower thickness.

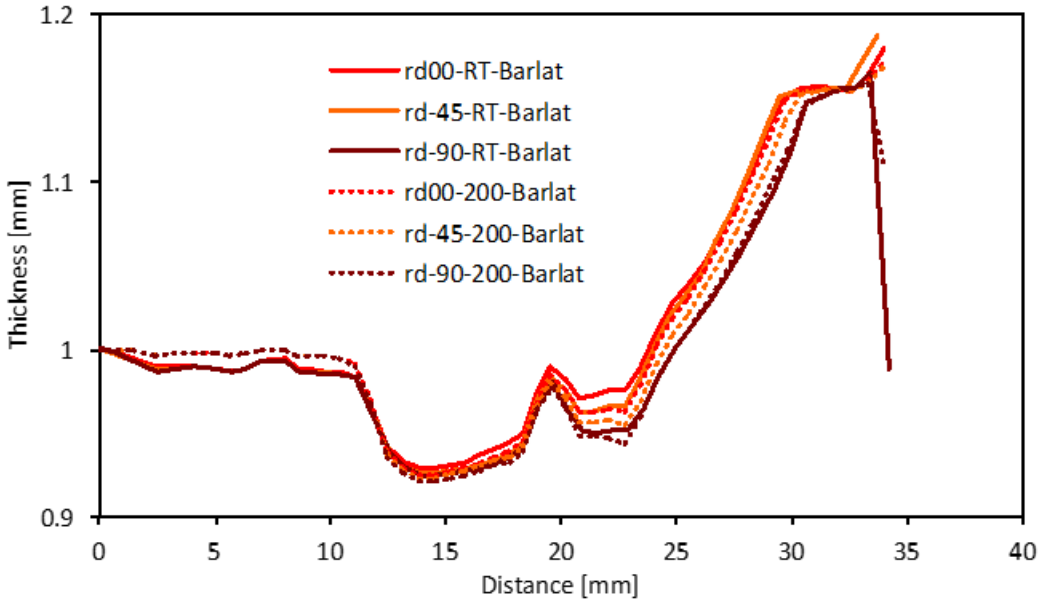

Figure 4.17 - Thickness evolution along the cup for RT and 200ºC for the 6061-T6 alloy.

Regarding the 6061-T6 alloy, Figure 4.17 presents the thickness distributions for RT and 200ºC, both for a friction coefficient of 0.10. In this case the influence of temperature is quite small. Compared with the 6016-T4 alloy, for which the cup's bottom has the lower thickness at 200ºC, the 6061-T6 alloy presents the opposite behaviour, with no change of thickness at 200ºC. At the cup's end, both temperatures present a zone that was crushed before the loss of contact with the blank-holder, being much more evident at RT. In this case, this effect occurs at the TD, for both temperatures.

4.3.3. Influence of temperature in ears profile

Figure 4.18 presents the ears profiles predicted for 6016-T4 alloy. As for the other results, the results obtained with a friction value of 0.15 is also presented, to allow a better comparison between numerical results. As expected, at 200ºC a slightly higher cup is formed. The ears profile obtained for 200ºC have the same trend, being the cup slightly higher for the 0.175 friction coefficient value. In this case, the squeezing of the cup's top (see Figure 4.16) seems to have a minor impact in the ears trend, which presents the typical valley at approximately 45º to RD. Also, since the Δr values are quite similar, the ears

profile, at RT and 200ºC, have the same trend. The increase of temperature leads to an increase of the cup's height.

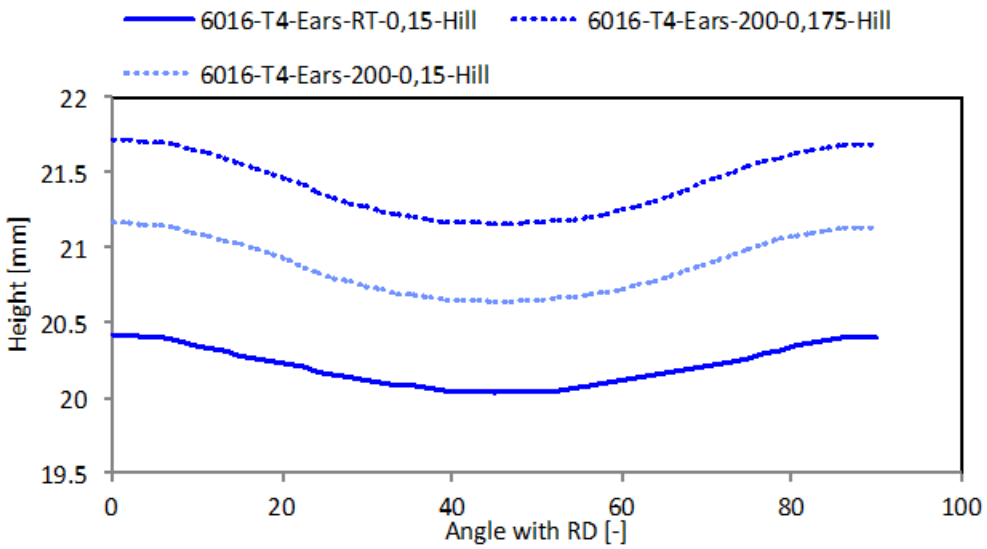

Figure 4.18 - Ears profile for RT and 200ºC for the 6016-T4 alloy.

For the 6061-T6 alloy, the same comparison was made considering the selected value of 0.10 for the friction coefficient, for both temperatures. As shown in Figure 4.19, the difference between RT and 200ºC is almost insignificant (the scale corresponds to a difference of 0.5 mm). Globally, the main difference is the cup's height being more uniform at 200ºC.

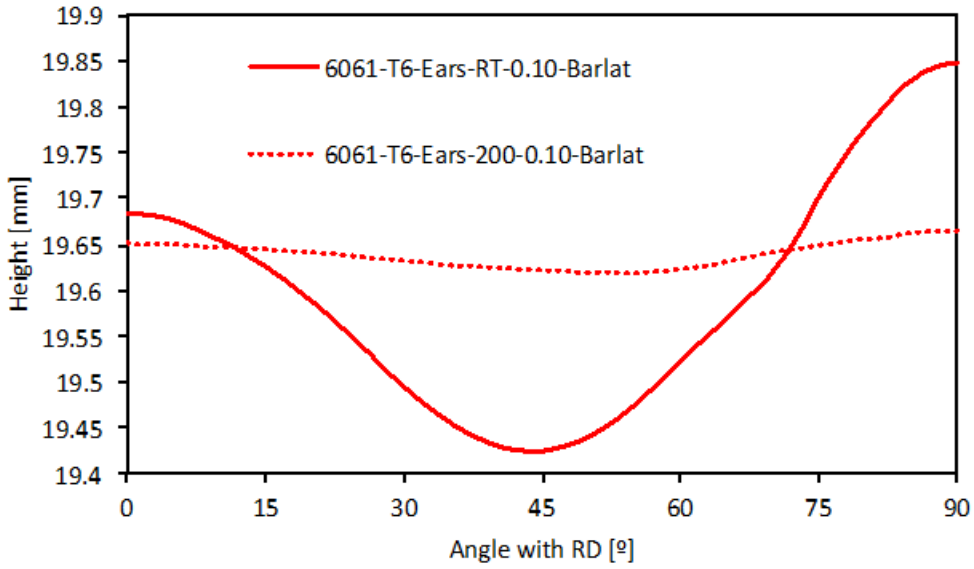

Figure 4.19 - Ears profile for RT and 200ºC for the 6061-T6 alloy.

4.4. Comparison between 6016-T4 and 6061-T6

The first comparison concerns the punch force evolution, at different temperatures for both alloys. As mentioned before, different frictions coefficients and yield criteria were used to both alloys. Table 4.9 presents the comparison between the two alloys for RT (6016-T4 alloy: 0.15 of friction coefficient with Hill'48; 6061-T6 alloy: 0.10 friction coefficient with Barlat'91). In the numerical results, the maximum punch force values are always attained by the 6061-T6. This is a result from the fact that the ironing force is always overestimated for this alloy.

Table 4.9 – 6061-T6 vs 6016-T4 punch force and ironing reduction at RT.

Temperature [25ºC]	6061-T6	6016-T4
Max punch force in deep drawing [kN]	27.56	20.58
Reduction [kN]	-	6.98
Reduction	-	25%
Max punch force in ironing phase [kN]	17.86	15.57
Reduction [kN]	-	2.29
Reduction	-	13%

Regarding the 200ºC, the values for the reduction in the punch force during the drawing and the ironing phases are presented in Table 4.10. Also, in this case the maximum values are always attained with the 6061-T6 alloy. However, since the influence of temperature is more effective for the 6061-T6 alloy the differences between both alloys reduce.

Table 4.10 – 6061-T6 vs 6016-T4 punch force and ironing reduction at 200ºC.

Temperature [200ºC]	6061-T6	6016-T4
Max punch force in deep drawing [kN]	17.77	13.67
Reduction [kN]	-	4.10
Reduction	-	23%
Max punch force in ironing phase [kN]	10.80	9.35
Reduction [kN]	-	1.45
Reduction	-	13%

The reported differences can be explained due to the fact that the blank-holder applies a constant force of 6kN until it loses contact with the blank, which only occurs when the last is fully drawn into the die cavity. Thus, before losing contact the blank-holder force is distributed along the flange, in the areas that presented higher thickness values. These zones will be the ones presenting localized deformation at the end of the forming process. This effect is very local, as it is shown in Figure 4.20, but it also influences the ironing stage, since it contributes to an increase of the thickness in the areas close to the one that is squeezed by the blank-holder. At the end of the forming process it is possible to observe that typically the direction presenting higher values of equivalent plastic strain, is related with the squeezing process. For the 6016-T4, the squeezing occurs both close to RD and TD. For the 6061-T6 the squeezing is noticeable mostly along TD (see also Figure 4.19). Typically the increase of the equivalent plastic strain is smaller at 200ºC, since the material presents lower flow stress values. When comparing both materials, the 6061-T6 presents always a more uniform distribution of the equivalent plastic strain, indicating a more isotropic behaviour.

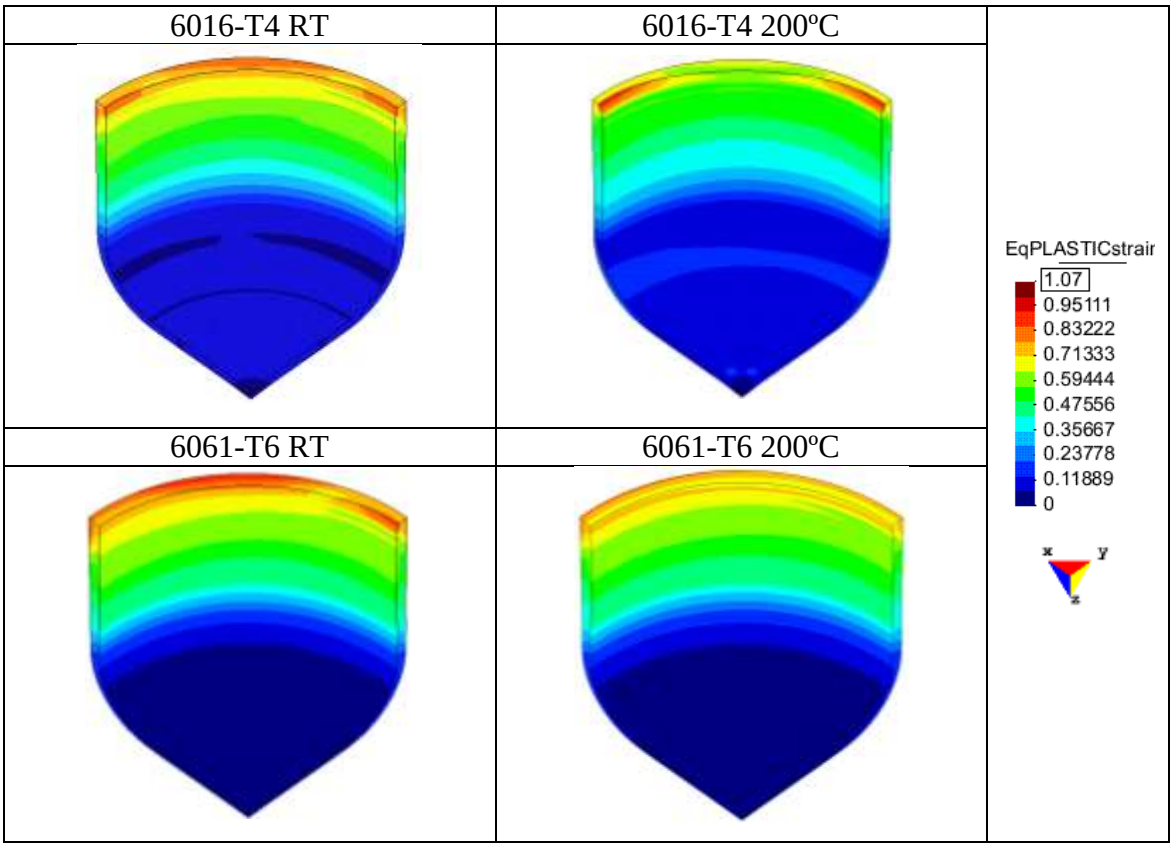

Figure 4.20 – 6061-T6 vs 6016-T4 equivalent plastic strain distribution at RT and 200ºC.

Concerning the thicknesses comparison they are related with the ears formation, and, as well, with the *r*-value. By definition (see Equation 2.2), if the *r*-value is higher along a certain direction this means that the material presents smaller tendency to deform in the thickness direction. When the analysis of the influence of the *r*-value is done along the flange, due to the compression state in the circumferential direction that is typical of this zone, the *r*-value determined with a tensile test along RD will characterize the behaviour of the material along TD and *vice-versa*. Figure 4.21 presents four cups, two for each alloy, for a punch displacement of 16mm, just before the loss of contact between the blank-holder with the blank, to be easier to see the thinning and thickening distribution before any crush or ironing occur. Since the 6061-T6 presents a lower *r*-value along TD, the material presents a higher thickening in the flange along the RD, as shown in Figure 4.21. This is also true for the 6016-T4 for the RT, while for 200ºC the distribution is more similar for both directions. Globally, as the 6016-T4 has lower *r*-values when compared with 6061-T6, this will lead to higher cups. However, it should be mentioned that also a lower friction coefficient was used for the 6061-T6. Figure 4.21 also highlights the differences previously shown for the thickness evolution along the cup, for the 6016-T4 alloy. The numerical results indicate that for RT and 200ºC the cup's bottom starts to deform from the beginning of the drawing process, leading to a lower thickness. This is certainly related with the material properties but also with the high value of friction coefficient used in this case.

The earing phenomenon results from both the *r*-values and the yield stress distribution in the sheet's plane. However, as previously mentioned in this example the ears profile is also been affected by the interaction with the blank-holder. Figure 4.22 presents the comparison for both alloys, regarding the ears profile. As expected, as the 6016-T4 as a lower yield stress, the force of the blank-holder has more impact, causing more stretching creating higher cups. Also, higher friction coefficients values were used in this case, contributing to an increase of these effects. All these factors influence the thickness distribution, highlighting the material anisotropic behaviour and, consequently, the ears profile. Thus, the 6061-T6 presents a more isotropic behaviour.

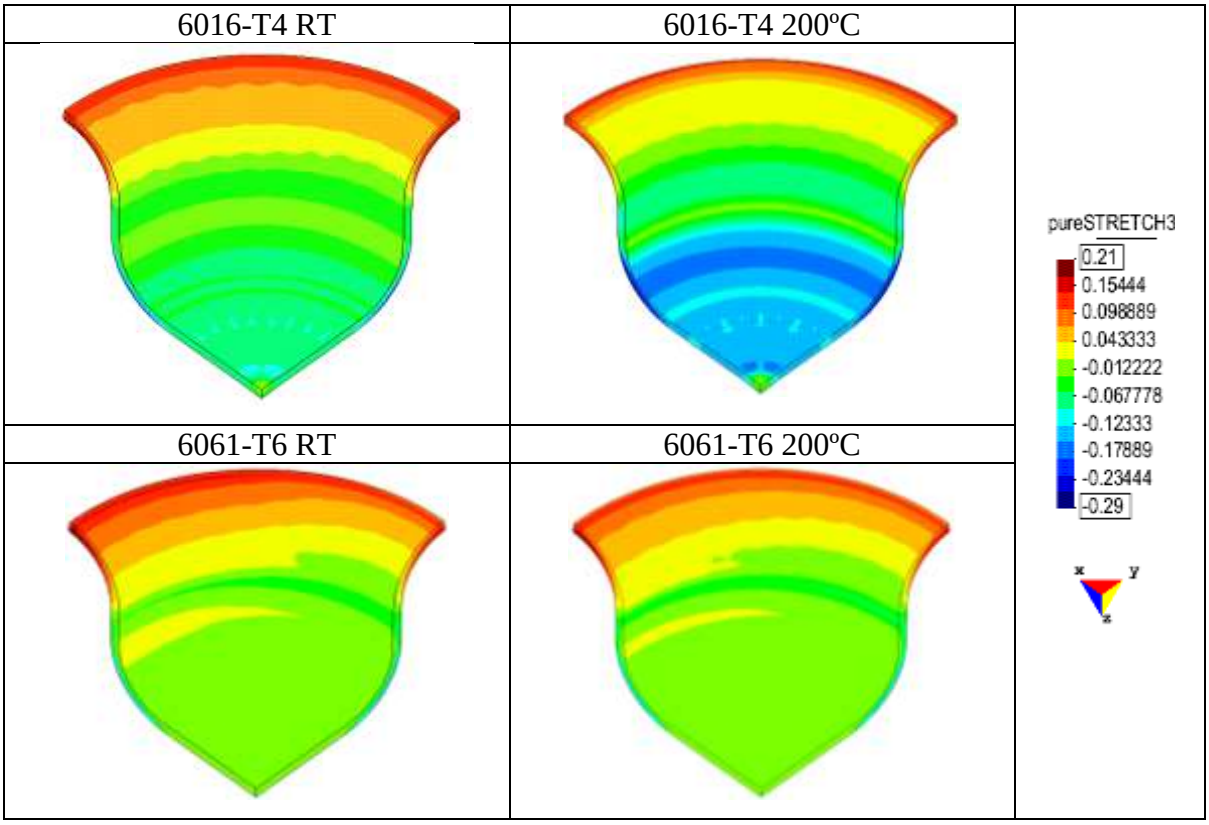

Figure 4.21 – 6061-T6 vs 6016-T4 pure stretch in the thickness direction distribution at RT and 200ºC.

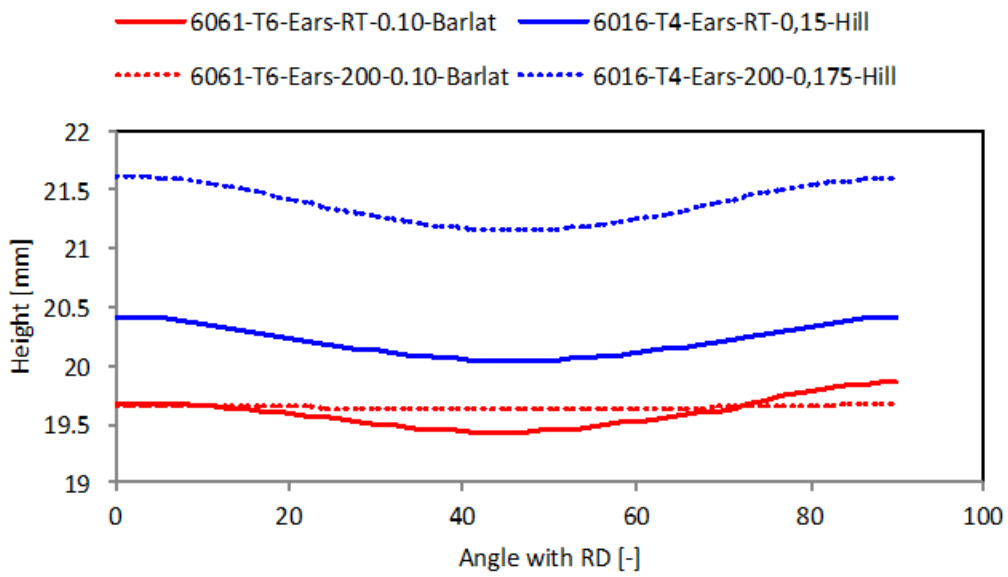

Figure 4.22 - Ears profile for RT and 200ºC for the 6016-T4 and 6061-T6 alloy.

4.1. Comparison between numerical simulation and experimental values

In this section, the comparison between numerical and experimental results is performed for both alloys, trying to have a perception about the requirements necessary to improve the numerical analysis.

The comparison of Table 3.10 and Table 4.9 shows that regarding the maximum punch force in the deep drawing phase, the 6061-T6 alloy presents a very similar value of force, and when compared with the 6016-T4, the same value of reduction is achieved. Concerning the ironing phase, the value of reduction is similar, around 10%, but in the numerical data is the 6061-T6 alloy that reaches the highest force value. Even though the ironing phase always presents higher numerical values of force, the amplitude of the reduction due to the influence of temperature is the same for the experimental and the numerical results.

The estimative of the global friction coefficient based on numerical results can be influencing this results, since for the for the 6016-T4 alloy the values were 0.150 for RT and 0.175 for 200ºC. Previous results obtained for the 5754-O lead to an estimate of 0.090, which is much closer to the one obtained for the 6061-T6 alloy (friction coefficient of 0.100). All these estimates were made based on the drawing force, and indicate that the experimental friction value tends to decrease for the ironing phase. Nevertheless, although the numerically predicted force reduction values with temperature do not match the experimental ones, the values are closer for the 6061-T6.

The experimental data concerning the thickness distribution in the cup begins only at 8mm due to the hole made in the cup's bottom in order to fix it to the measurement platform. Figure 4.23 presents the results for the 6016-T4, at RT and 200ºC. The reason why the experimental data has higher values in the cup's bottom results from the higher initial thickness (1.04mm). As expected and mentioned before, at 200ºC, the experimental results show that at this temperature the thickness is globally higher, as the material flows better. This does not happens in the numerical results, since the cup's bottom at 200ºC suffers high strains (see Figure 4.21), reversing the trend between temperatures. Also, in the numerical results, the crush that the blank suffers from the loss of contact with the blank-holder reaches higher values for both temperatures. This can be explained by the high value adopted for the friction coefficient, which is constant in the numerical

simulations, while in the experimental tests it can change with parameters such as the contact pressure, the temperature and the flow stress of the material. Also, the fact that the loss of contact with the blank-holder is occurring for higher values of punch displacement is an indicator that the material in the numerical simulation is not flowing as expected by the experimental results.

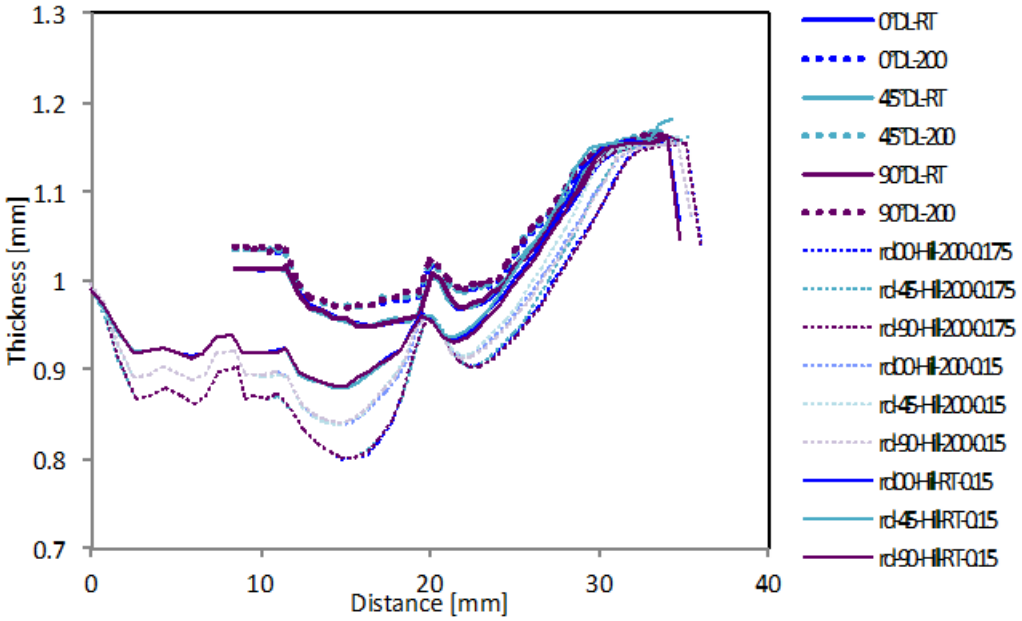

Figure 4.23 – Thickness comparison between the numerical and experimental results for the 6016-T4 alloy, at RT and 200ºC.

The results for the 6061-T6, at RT and 200ºC, are presented in Figure 4.24. Regarding the experimental data, the initial thickness of the blanks acquires lower values than for 6016-T4, being closer to 1mm. In this case, the trends for both types of results are quite similar. At 200ºC, as the material have a better flow behaviour, consequently, the thickness attains globally slightly higher values, being this effect more visible for the experimental data. In fact, it seems that the flow behaviour is accurately represented by the numerical model, since the loss of contact between the blank-holder and the blank occur for approximately the same displacement. However, the crush at the cup's top is one more time highlighted by the numerical procedure, although with less amplitude than for the 6016-T4 alloy. It is important to mention that for the 6016-T4, the squeezing is never visible in the experimental cups.

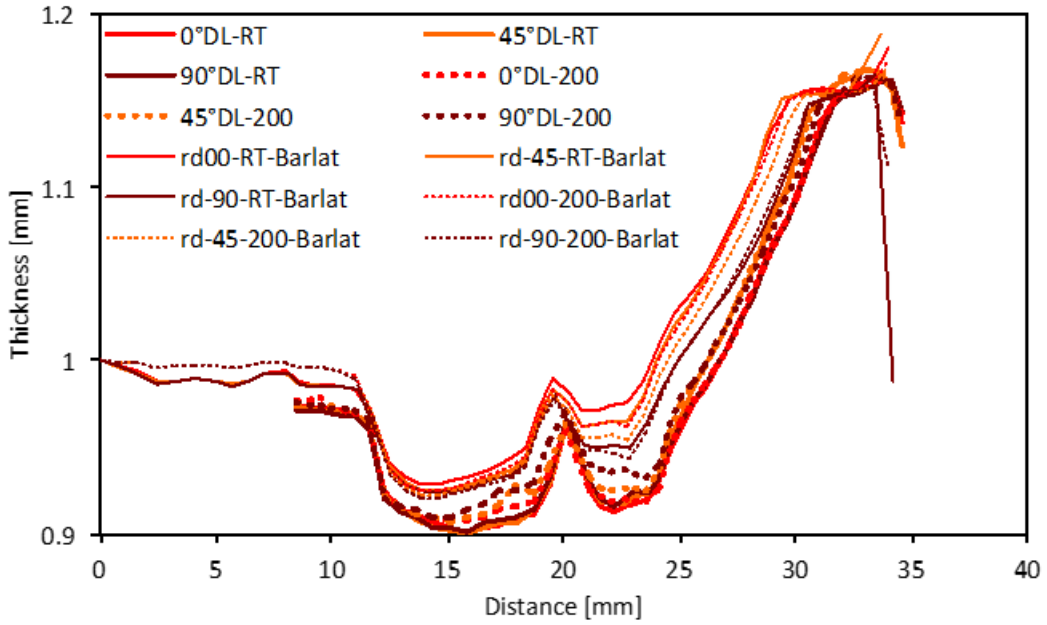

Figure 4.24 – Thickness comparison between the numerical and experimental results for 6he 6061-T6 alloy, at RT and 200ºC.

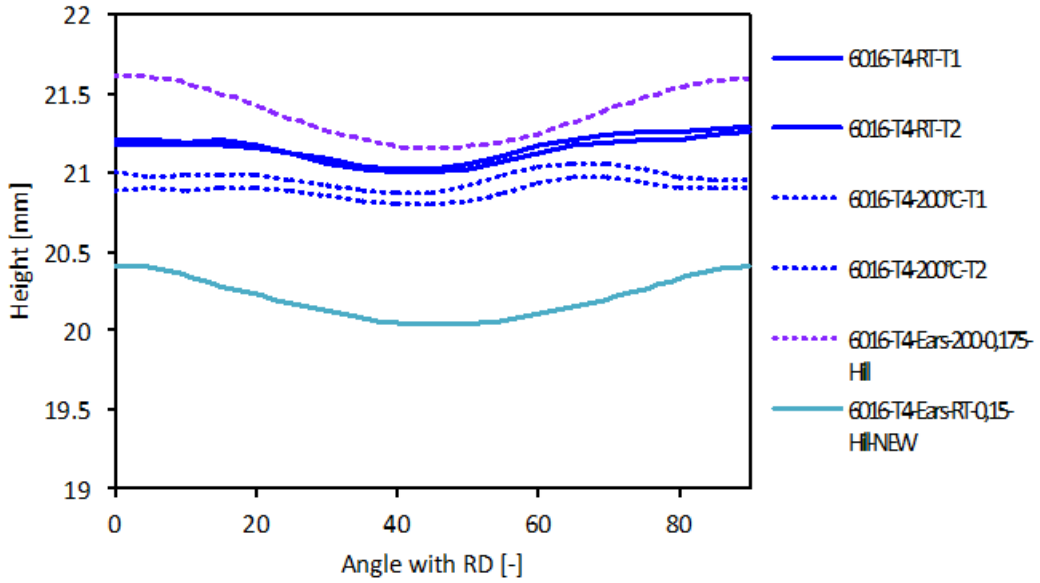

Figure 4.25 - Comparison of ears profile between experimental and numerical analysis at RT and 200ºC for 6016-T4.

Figure 4.25 compares the ears profiles obtained for the 6016-T4 alloy. It is interesting to note that the global cup's height is underestimated by the experimental results for RT, while it is overestimated for 200'C. This results in a different trend for the

influence of temperature on the ears profile, predicted experimentally and numerically. Also, the anisotropy exhibited by the numerical results is more significant.

Regarding the 6061-T6 alloy the results are shown in Figure 4.26. For this alloy the numerical and experimental trends are quite similar. The more noticeable difference is in the cup's height, which is always higher in the experimental results. As previously mentioned, this can be explained by the use of a constant friction coefficient in the numerical model.

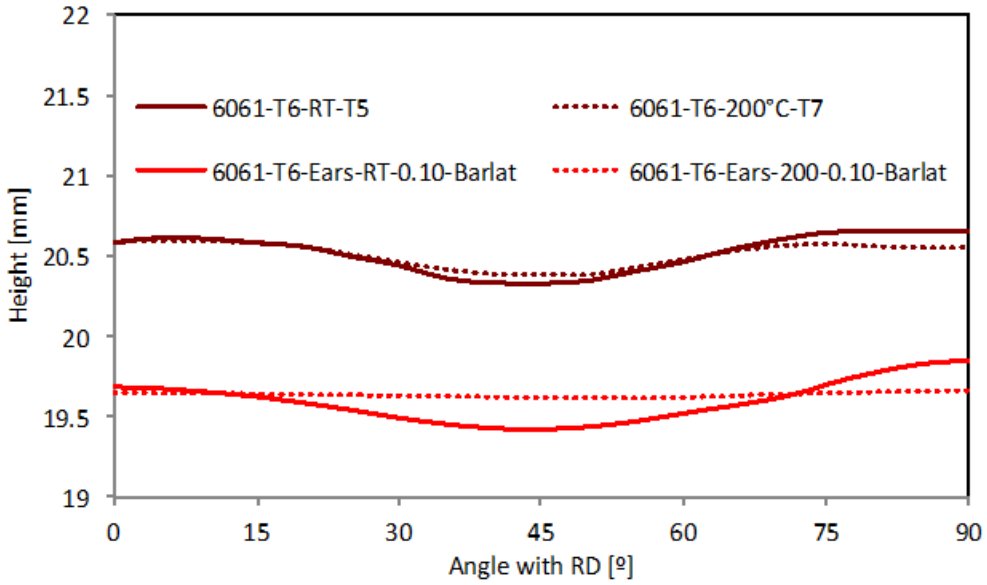

Figure 4.26 - Comparison of ears profile between experimental and numerical analysis at RT and 200ºC for 6061-T6.

5. CONCLUSION

Regarding the experimental analysis, the results indicate that the increase of temperature to 200ºC contributes for: (i) lower forces, for both drawing and ironing phases; (ii) higher thickness along the cup, indicating an improvement of the material flow; (iii) lower springback values. Regarding the springback, the reduction for 6016-T4 is smaller because the overture at RT is approximately 5 mm, while for the 6061-T6 is almost the double. In fact, the temperature seems to have the highest influence for the 6061-T6, although 5754-O has better values regarding the maximum punch force in both phases, and 6016-T4 achieves the lowest springback values.

One of the main drawbacks about the warm forming process is the time necessary to heat the blank until the 200ºC. During this time the blank is in contact with the die and the blank-holder, while the punch is cooled through air, working against the increase of temperature. This occurs mainly because of the leak of air between the ejector and the punch. The 6061-T6 alloy seems to have a lower conductivity coefficient since it always required more time to attain the 200ºC (~30 minutes). This time is influence by the sequence of the tests. In fact, it was observed that it is very hard to attain the 200ºC in the blank when the test starts with a cold die and blank-holder. Thus, it is recommended to perform a trial-test, because although the blank does not attains 200ºC it will warm the tools. In fact, in order to attain the 200ºC in the blank it is necessary to reach approximately 230ºC in the die. Also, during the heating process it seems that the lubricant starts to lose some properties, which can contribute to decrease the flow of the blank into the die's cavity.

Regarding the numerical analysis, the biggest difficulty was to have constitutive material parameters for both materials. Although not presented in the text, a preliminary study was performed considering constitutive parameters identified for the 6061, but with a different heat treatment (T4 instead of T6). This option was adopted because the experimental test reported in section 3.1 were being performed simultaneously. However, it was observed that the heat treatment has a strong impact in the 6061 alloy mechanical properties. The parameters identification was performed based on the tensile tests results, which attain the maximum punch force for very low values of strain,

particularly for the 6061-T6 alloy. The yield criteria were identified based also only in the tensile tests results, which lead to very similar yield surfaces for the Hill'48 and the Barlat'91. Based on previous results, the global friction coefficient was best fitted by trial and error, using has reference the drawing force evolution. However, for the 6016-T4 this lead to a much higher value of friction coefficient. For each alloy and temperature, the best combination between the yield criterion and friction coefficient was also found using a trial and error approach.

The results also show that the ears profile, as well as the thickness at the cup's top is being strongly influenced by the crush that the blank suffer at the final contact with the blank-holder. This strongly decrease the thickness, locally, but also contributes for increasing the thickness in the surrounding area. Thus, this effect also influences the amount of blank subsequently submitted to ironing. The ears profile is a result of the material anisotropic behaviour but mainly of the crush. In order to minimize this event, the used of a stopper between the die and the blank-holder can help to prevent the crush, and so, the ears profile would be consequence of the anisotropy, matching the *r*-values of each alloy. Another possible approach is to perform the numerical simulations considering a deformable blank-holder, which would minimize the local effects in the blank.

BIBLIOGRAPHY

Alves, 2003 - J.L. Alves, (2013). Simulação numérica do processo de estampagem de chapas metálicas – modelação mecânica e métodos numéricos, PHD Thesis, Department of Mechanical Engineering, University of Minho, Gimarães, Portugal.

Barlat et al., 1991 - Barlat, Frédéric, Daniel J. Lege, John C. Brem, 1991. A six-component yield function for anisotropic materials. International Journal of Plasticity 7, n. 7 : 693–712. doi:10.1016/0749-6419(91)90052-Z.

Burger et al., 1995 - Burger G.B., Gupta A.K., Jeffrey P.W., Lloyd D.J., 1995. Microstructural control of aluminium sheet used in automotive applications. Materials Characterization 35, 23–39.

Chen et al., 2005 – Chen, X.M., Shi, M.F., Ren, F., Xia, Z.C., 2005. Springback Prediction on Slit-Ring Test, in: AIP CONFERENCE PROCEEDINGS. IOP INSTITUTE OF PHYSICS PUBLISHING LTD, p. 222.

Cobden et al., 1994 - Cobden R., Alcan, Banbury, 1974. Alluminum: Physical Properties, Characteristics and Alloys. TALAT Lecture 1501.

Coër, 2013 – Coër J., (2013). Mise en forme par emboutissage en température d'un alliage d'aluminium AA5754-O. Thèse/Université Bretagne Sud.

Fridlyander et al., 2002 - Fridlyander, I. N., V. G. Sister, O. E. Grushko, V. V. Berstenev, L. M. Sheveleva, e L. A. Ivanova, 2002. Aluminum Alloys: Promising Materials in the Automotive Industry. Metal Science and Heat Treatment 44, n. 9–10 (1 de Setembro de 2002): 365–70. doi:10.1023/A:1021901715578.

Ghosh, 2011– Ghosh M., 2011. Microstructurally Controlled Mechanical Properties of Al-Mg-Si Alloys for Warm Forming Applications. PhD Thesis.

Ghosh et al., 2014 - Ghosh M., Miroux A., Werkhoven R.J., Bolt P.J., Kestens L.A.I., 2014. Warm deep-drawing and post drawing analysis of two Al–Mg–Si alloys. Journal of Materials Processing Technology 214, 756–766. doi:10.1016/j.jmatprotec.2013.10.020

Habraken et al., 1995 - Habraken, F. A. C. M., J. H. Dautzenberg, 1995. Some Applications of the Barlat 1991 Yield Criterion. CIRP Annals - Manufacturing Technology 44, n. 1 :185–88. doi:10.1016/S0007-8506(07)62303-8.

Jin et al., 2011 - Jin, Shun Yi, e William Altenhof. Control of load/displacement responses of AA6061-T6 and T4 circular extrusions under axial compressive loads. International Journal of Impact Engineering 38, n. 1 (Janeiro de 2011): 1–12. doi:10.1016/j.ijimpeng.2010.09.001.

Laurent et al., 2009 - Laurent, H., Grèze, R., Manach, P.Y., Thuillier, S., 2009. Influence of constitutive model in springback prediction using the split-ring test. International Journal of Mechanical Sciences 51, 233–245.

doi:10.1016/j.ijmecsci.2008.12.010

Lee et al., 2014 - Lee, Woei-Shyan, e Zih-Chao Tang, 2014. Relationship between mechanical properties and microstructural response of 6061-T6 aluminium alloy impacted at elevated temperatures. Materials & Design 58 (Junho de 2014): 116–24. doi:10.1016/j.matdes.2014.01.053.

Mahathaninwong, 2012 - Mahathaninwong N., Plookphol T., Wannasin J., Wisutmethangoon S., 2012. T6 heat treatment of rheocasting 7075 Al alloy. Materials Science and Engineering: A 532 (15 de Janeiro de 2012): 91–99. doi:10.1016/j.msea.2011.10.068.

Malavolta, 2008 – Malavolta Alexandre T., 2008. Metodologia para determinação dos parâmetros utilizados em uma nova superfície de escoamento anisotrópica para processos de conformação de chapas metálicas. Tese/Universidade de São Paulo.

Moon et al., 2003 - Moon, Y.H., Kang, S.S., Cho, J.R., Kim, T.G., 2003. Effect of tool temperature on the reduction of the springback of aluminium sheets. Journal of Materials Processing Technology 132, 365–368. doi:10.1016/S0924-0136(02)00925-1

Oliveira et al,. 2007 - Oliveira, M.C., Alves, J.L., Chaparro, B.M., Menezes, L.F., 2007. Study on the influence of work-hardening modeling in springback prediction. International Journal of Plasticity, NUMISHEET2005 Conference 23, 516–543. doi:10.1016/j.ijplas.2006.07.003

Park, 1986 - Park Bom K., 1986. Aluminum 6XXX alloy products of high strength and toughness having stable response to high temperature artificial aging treatments and method for producing. US 4589932 (A) - 1986-05-20.

Raju et al., 2010 - Raju, S., Ganesan, G., Karthikeyan, R., 2010. "Influence of variables in deep drawing of AA 6061 sheet", Transactions of Nonferrous Metals Society of China 20, 1856–1862. doi:10.1016/S1003-6326(09)60386-1.

Ramesh et al., 2013 - Ramesh, G., Reddy, G.C.M., 2013. Analysis of Optimization of Blank Holding Force In Deep Drawing By Using LS DYNA. Analysis 3, 1975–1995.

Rashkeev et al., 2002 - Rashkeev, Sergey N., Michael V. Glazov, e Frédéric Barlat, 2002. Strain-rate sensitivity limit diagrams and plastic instabilities in a 6xxx series aluminium alloy Part I: Analysis of temporal stress–strain serrations. Computational materials science 24, n. 3: 295–309.

Reddy et al., 2012 - Reddy, R.V., Reddy, D.T.J., Reddy, D.G., n.d. Effect of Various Parameters on the Wrinkling In Deep Drawing Cylindrical Cups. International Journal of Engineering Trends and Technology, Volume3 53–58.

Simões, 2012 - Simões Vasco M., 2012. Analysis of the influence of process parameters in the deep drawing of a cylindrical cup. Tese/Universidade de Coimbra.

Simões et al., 2013 - Simões Vasco M., Coër Jérémy, Laurent Hervé, Oliveira Marta C., Alves José L., Manach Pierre Y., Menezes Luís F., 2013. Influence of the yield criteria in the numerical simulation of an AA5745-O cylindrical cup. Congreso de Métodos Numéricos en Ingeniería 25-28 junio 2013, Bilbao, España

TN, 2004 - Tecnologia Naval. Materiais Metálicos 2003-2004, Parte III.

van den Boogaard et. al, 2006 - A.H. van den Boogaard, J. Huétink, Simulation of aluminium sheet forming at elevated temperatures, Computer Methods in Applied Mechanics and Engineering, Vol 195, pp 6691–6709, (2006).

ANNEX A

MAXIMUM TEMPERATURE RANGE
Thermocouple Grade
– 328 to 2282°F
– 200 to 1250°C
Extension Grade
32 to 392°F
0 to 200°C
LIMITS OF ERROR
(whichever is greater)
Standard: 2.2°C or 0.75% Above 0°C
2.2°C or 2.0% Below 0°C
Special: 1.1°C or 0.4%
COMMENTS, BARE WIRE ENVIRONMENT:
Clean Oxidizing and Inert; Limited Use in Vacuum or Reducing; Wide Temperature Range; Most Popular Calibration
TEMPERATURE IN DEGREES °C
REFERENCE JUNCTION AT 0°C

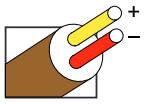

Thermocouple Grade

Nickel-Chromium vs. Nickel-Aluminum

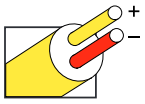

Extension Grade

Revised Thermocouple Reference Tables

TYPE K
Reference Tables N.I.S.T. Monograph 175 Revised to ITS-90

Z

Thermoelectric Voltage in Millivolts

°C	-10	-9	-8	-7	-6	-5	-4	-3	-2	-1	0	°C
-260	-6.458	-6.457	-6.456	-6.455	-6.453	-6.452	-6.450	-6.448	-6.446	-6.444	-6.441	-260
-250	-6.441	-6.438	-6.435	-6.432	-6.429	-6.425	-6.421	-6.417	-6.413	-6.408	-6.404	-250
-240	-6.404	-6.399	-6.393	-6.388	-6.382	-6.377	-6.370	-6.364	-6.358	-6.351	-6.344	-240
-230	-6.344	-6.337	-6.329	-6.322	-6.314	-6.306	-6.297	-6.289	-6.280	-6.271	-6.262	-230
-220	-6.262	-6.252	-6.243	-6.233	-6.223	-6.213	-6.202	-6.192	-6.181	-6.170	-6.158	-220
-210	-6.158	-6.147	-6.135	-6.123	-6.111	-6.099	-6.087	-6.074	-6.061	-6.048	-6.035	-210
-200	-6.035	-6.021	-6.007	-5.994	-5.980	-5.965	-5.951	-5.936	-5.922	-5.907	-5.891	-200
-190	-5.891	-5.876	-5.861	-5.845	-5.829	-5.813	-5.797	-5.780	-5.763	-5.747	-5.730	-190
-180	-5.730	-5.713	-5.695	-5.678	-5.660	-5.642	-5.624	-5.606	-5.588	-5.569	-5.550	-180
-170	-5.550	-5.531	-5.512	-5.493	-5.474	-5.454	-5.435	-5.415	-5.395	-5.374	-5.354	-170
-160	-5.354	-5.333	-5.313	-5.292	-5.271	-5.250	-5.228	-5.207	-5.185	-5.163	-5.141	-160
-150	-5.141	-5.119	-5.097	-5.074	-5.052	-5.029	-5.006	-4.983	-4.960	-4.936	-4.913	-150
-140	-4.913	-4.889	-4.865	-4.841	-4.817	-4.793	-4.768	-4.744	-4.719	-4.694	-4.669	-140
-130	-4.669	-4.644	-4.618	-4.593	-4.567	-4.542	-4.516	-4.490	-4.463	-4.437	-4.411	-130
-120	-4.411	-4.384	-4.357	-4.330	-4.303	-4.276	-4.249	-4.221	-4.194	-4.166	-4.138	-120
-110	-4.138	-4.110	-4.082	-4.054	-4.025	-3.997	-3.968	-3.939	-3.911	-3.882	-3.852	-110
-100	-3.852	-3.823	-3.794	-3.764	-3.734	-3.705	-3.675	-3.645	-3.614	-3.584	-3.554	-100
-90	-3.554	-3.523	-3.492	-3.462	-3.431	-3.400	-3.368	-3.337	-3.306	-3.274	-3.243	-90
-80	-3.243	-3.211	-3.179	-3.147	-3.115	-3.083	-3.050	-3.018	-2.986	-2.953	-2.920	-80
-70	-2.920	-2.887	-2.854	-2.821	-2.788	-2.755	-2.721	-2.688	-2.654	-2.620	-2.587	-70
-60	-2.587	-2.553	-2.519	-2.485	-2.450	-2.416	-2.382	-2.347	-2.312	-2.278	-2.243	-60
-50	-2.243	-2.208	-2.173	-2.138	-2.103	-2.067	-2.032	-1.996	-1.961	-1.925	-1.889	-50
-40	-1.889	-1.854	-1.818	-1.782	-1.745	-1.709	-1.673	-1.637	-1.600	-1.564	-1.527	-40
-30	-1.527	-1.490	-1.453	-1.417	-1.380	-1.343	-1.305	-1.268	-1.231	-1.194	-1.156	-30
-20	-1.156	-1.119	-1.081	-1.043	-1.006	-0.968	-0.930	-0.892	-0.854	-0.816	-0.778	-20
-10	-0.778	-0.739	-0.701	-0.663	-0.624	-0.586	-0.547	-0.508	-0.470	-0.431	-0.392	-10
0	-0.392	-0.353	-0.314	-0.275	-0.236	-0.197	-0.157	-0.118	-0.079	-0.039	0.000	0
0	0.000	0.039	0.079	0.119	0.158	0.198	0.238	0.277	0.317	0.357	0.397	0
10	0.397	0.437	0.477	0.517	0.557	0.597	0.637	0.677	0.718	0.758	0.798	10
20	0.798	0.838	0.879	0.919	0.960	1.000	1.041	1.081	1.122	1.163	1.203	20
30	1.203	1.244	1.285	1.326	1.366	1.407	1.448	1.489	1.530	1.571	1.612	30
40	1.612	1.653	1.694	1.735	1.776	1.817	1.858	1.899	1.941	1.982	2.023	40
50	2.023	2.064	2.106	2.147	2.188	2.230	2.271	2.312	2.354	2.395	2.436	50
60	2.436	2.478	2.519	2.561	2.602	2.644	2.685	2.727	2.768	2.810	2.851	60
70	2.851	2.893	2.934	2.976	3.017	3.059	3.100	3.142	3.184	3.225	3.267	70
80	3.267	3.308	3.350	3.391	3.433	3.474	3.516	3.557	3.599	3.640	3.682	80
90	3.682	3.723	3.765	3.806	3.848	3.889	3.931	3.972	4.013	4.055	4.096	90
100	4.096	4.138	4.179	4.220	4.262	4.303	4.344	4.385	4.427	4.468	4.509	100
110	4.509	4.550	4.591	4.633	4.674	4.715	4.756	4.797	4.838	4.879	4.920	110
120	4.920	4.961	5.002	5.043	5.084	5.124	5.165	5.206	5.247	5.288	5.328	120
130	5.328	5.369	5.410	5.450	5.491	5.532	5.572	5.613	5.653	5.694	5.735	130
140	5.735	5.775	5.815	5.856	5.896	5.937	5.977	6.017	6.058	6.098	6.138	140
150	6.138	6.179	6.219	6.259	6.299	6.339	6.380	6.420	6.460	6.500	6.540	150
160	6.540	6.580	6.620	6.660	6.701	6.741	6.781	6.821	6.861	6.901	6.941	160
170	6.941	6.981	7.021	7.060	7.100	7.140	7.180	7.220	7.260	7.300	7.340	170
180	7.340	7.380	7.420	7.460	7.500	7.540	7.579	7.619	7.659	7.699	7.739	180
190	7.739	7.779	7.819	7.859	7.899	7.939	7.979	8.019	8.059	8.099	8.138	190
200	8.138	8.178	8.218	8.258	8.298	8.338	8.378	8.418	8.458	8.499	8.539	200
210	8.539	8.579	8.619	8.659	8.699	8.739	8.779	8.819	8.860	8.900	8.940	210
220	8.940	8.980	9.020	9.061	9.101	9.141	9.181	9.222	9.262	9.302	9.343	220
230	9.343	9.383	9.423	9.464	9.504	9.545	9.585	9.626	9.666	9.707	9.747	230
240	9.747	9.788	9.828	9.869	9.909	9.950	9.991	10.031	10.072	10.113	10.153	240
°C	0	1	2	3	4	5	6	7	8	9	10	°C

°C	0	1	2	3	4	5	6	7	8	9	10	°C
250	10.153	10.194	10.235	10.276	10.316	10.357	10.398	10.439	10.480	10.520	10.561	250
260	10.561	10.602	10.643	10.684	10.725	10.766	10.807	10.848	10.889	10.930	10.971	260
270	10.971	11.012	11.053	11.094	11.135	11.176	11.217	11.259	11.300	11.341	11.382	270
280	11.382	11.423	11.465	11.506	11.547	11.588	11.630	11.671	11.712	11.753	11.795	280
290	11.795	11.836	11.877	11.919	11.960	12.001	12.043	12.084	12.126	12.167	12.209	290
300	12.209	12.250	12.291	12.333	12.374	12.416	12.457	12.499	12.540	12.582	12.624	300
310	12.624	12.665	12.707	12.748	12.790	12.831	12.873	12.915	12.956	12.998	13.040	310
320	13.040	13.081	13.123	13.165	13.206	13.248	13.290	13.331	13.373	13.415	13.457	320
330	13.457	13.498	13.540	13.582	13.624	13.665	13.707	13.749	13.791	13.833	13.874	330
340	13.874	13.916	13.958	14.000	14.042	14.084	14.126	14.167	14.209	14.251	14.293	340
350	14.293	14.335	14.377	14.419	14.461	14.503	14.545	14.587	14.629	14.671	14.713	350
360	14.713	14.755	14.797	14.839	14.881	14.923	14.965	15.007	15.049	15.091	15.133	360
370	15.133	15.175	15.217	15.259	15.301	15.343	15.385	15.427	15.469	15.511	15.554	370
380	15.554	15.596	15.638	15.680	15.722	15.764	15.806	15.849	15.891	15.933	15.975	380
390	15.975	16.017	16.059	16.102	16.144	16.186	16.228	16.270	16.313	16.355	16.397	390
400	16.397	16.439	16.482	16.524	16.566	16.608	16.651	16.693	16.735	16.778	16.820	400
410	16.820	16.862	16.904	16.947	16.989	17.031	17.074	17.116	17.158	17.201	17.243	410
420	17.243	17.285	17.328	17.370	17.413	17.455	17.497	17.540	17.582	17.624	17.667	420
430	17.667	17.709	17.752	17.794	17.837	17.879	17.921	17.964	18.006	18.049	18.091	430
440	18.091	18.134	18.176	18.218	18.261	18.303	18.346	18.388	18.431	18.473	18.516	440
450	18.516	18.558	18.601	18.643	18.686	18.728	18.771	18.813	18.856	18.898	18.941	450
460	18.941	18.983	19.026	19.068	19.111	19.154	19.196	19.239	19.281	19.324	19.366	460
470	19.366	19.409	19.451	19.494	19.537	19.579	19.622	19.664	19.707	19.750	19.792	470
480	19.792	19.835	19.877	19.920	19.962	20.005	20.048	20.090	20.133	20.175	20.218	480
490	20.218	20.261	20.303	20.346	20.389	20.431	20.474	20.516	20.559	20.602	20.644	490
500	20.644	20.687	20.730	20.772	20.815	20.857	20.900	20.943	20.985	21.028	21.071	500
510	21.071	21.113	21.156	21.199	21.241	21.284	21.326	21.369	21.412	21.454	21.497	510
520	21.497	21.540	21.582	21.625	21.668	21.710	21.753	21.796	21.838	21.881	21.924	520
530	21.924	21.966	22.009	22.052	22.094	22.137	22.179	22.222	22.265	22.307	22.350	530
540	22.350	22.393	22.435	22.478	22.521	22.563	22.606	22.649	22.691	22.734	22.776	540
550	22.776	22.819	22.862	22.904	22.947	22.990	23.032	23.075	23.117	23.160	23.203	550
560	23.203	23.245	23.288	23.331	23.373	23.416	23.458	23.501	23.544	23.586	23.629	560
570	23.629	23.671	23.714	23.757	23.799	23.842	23.884	23.927	23.970	24.012	24.055	570
580	24.055	24.097	24.140	24.182	24.225	24.267	24.310	24.353	24.395	24.438	24.480	580
590	24.480	24.523	24.565	24.608	24.650	24.693	24.735	24.778	24.820	24.863	24.905	590
600	24.905	24.948	24.990	25.033	25.075	25.118	25.160	25.203	25.245	25.288	25.330	600
610	25.330	25.373	25.415	25.458	25.500	25.543	25.585	25.627	25.670	25.712	25.755	610
620	25.755	25.797	25.840	25.882	25.924	25.967	26.009	26.052	26.094	26.136	26.179	620
630	26.179	26.221	26.263	26.306	26.348	26.390	26.433	26.475	26.517	26.560	26.602	630
640	26.602	26.644	26.687	26.729	26.771	26.814	26.856	26.898	26.940	26.983	27.025	640
650	27.025	27.067	27.109	27.152	27.194	27.236	27.278	27.320	27.363	27.405	27.447	650
660	27.447	27.489	27.531	27.574	27.616	27.658	27.700	27.742	27.784	27.826	27.869	660
670	27.869	27.911	27.953	27.995	28.037	28.079	28.121	28.163	28.205	28.247	28.289	670
680	28.289	28.332	28.374	28.416	28.458	28.500	28.542	28.584	28.626	28.668	28.710	680
690	28.710	28.752	28.794	28.835	28.877	28.919	28.961	29.003	29.045	29.087	29.129	690
700	29.129	29.171	29.213	29.255	29.297	29.338	29.380	29.422	29.464	29.506	29.548	700
710	29.548	29.589	29.631	29.673	29.715	29.757	29.798	29.840	29.882	29.924	29.965	710
720	29.965	30.007	30.049	30.090	30.132	30.174	30.216	30.257	30.299	30.341	30.382	720
730	30.382	30.424	30.466	30.507	30.549	30.590	30.632	30.674	30.715	30.757	30.798	730
740	30.798	30.840	30.881	30.923	30.964	31.006	31.047	31.089	31.130	31.172	31.213	740
750	31.213	31.255	31.296	31.338	31.379	31.421	31.462	31.504	31.545	31.586	31.628	750
760	31.628	31.669	31.710	31.752	31.793	31.834	31.876	31.917	31.958	32.000	32.041	760
770	32.041	32.082	32.124	32.165	32.206	32.247	32.289	32.330	32.371	32.412	32.453	770
780	32.453	32.495	32.536	32.577	32.618	32.659	32.700	32.742	32.783	32.824	32.865	780
790	32.865	32.906	32.947	32.988	33.029	33.070	33.111	33.152	33.193	33.234	33.275	790
°C	0	1	2	3	4	5	6	7	8	9	10	°C

Z-204

Figure A 1- Revised Thermocouple Reference Tables.